RAPORT ŞTIINŢIFIC FINAL

The research team members who carried out research activities in the project "Fuzzy controllers for shape memory alloys systems", no. TE 65 / 2020, project code PN-III-P1-1.1-TE-2019-1117, http://www.aut.upt.ro/~claudia.dragos/TE2019.html, consists of: Lect. Claudia-Adina BOJAN-DRAGOŞ – Director of the project, Prof. Stefan PREITL – Member, Lect. Alexandra-Iulia SZEDLAK-STINEAN – Member, Assist. Raul-Cristian ROMAN – Member and M.Sc. Elena-Lorena HEDREA - Member.

A. Obiectivele prevăzute/realizate

The 1st Stage of the project – The analysis of the theoretical framework with regard to the improving of the existing control algorithms and to the development of new control algorithms to improve the control solutions for the processes that include SMA actuators *(In Romanian – Analiza cercetărilor teoretice actuale privind îmbunătăţirea soluţiilor de reglarea existente şi proiectarea de noi regulatoare pentru a îmbunătăţii performaţele sistemelor de reglare automată pentru procesele în legătură cu aliaje cu memoria formei)* – carried out during September-December 2020 has been fulfilled and is grouped in the form of the following activities:

Act 1.1 - The analysis of the state-of-the-art on theoretical research and practical applications on the laboratory equipment with SMA and on other laboratory equipment with SMA actuators *(In Romanian – Analiza cercetărilor teoretice actuale şi studierea aplicaţiilor experimentale pe echipamente de laborator în legătură cu SMA şi pe alte echipamente de laborator cu elemente de execuţie bazate pe SMA).* To accomplish this activity, the analysis of the state-of-the-art on theoretical research with regard to the existing control algorithms to control processes that include SMA actuators.

Shape Memory Alloys (SMA) are metallic materials, called "intelligent materials", with special features as high force-to-mass ratio, light weight, biocompatibility, clean and silent operation, which make them widely used as actuators in control systems (Mituletu et al., 2019; Kuang et al., 2015; Kim et al., 2013; Lagoudas, 2008; Mohd Jani et al., 2014; Senthilkumar, 2012). The literature analysis reveals that SMA actuator testing stands were designed in both simple cases to demonstrate the SMA behavior and complicated ones to model the specific processes and next design controllers including nonlinear robust ones for position and tracking control (Mituletu et al., 2019; Yang et al., 2019). SMA have some disadvantages such as low energy efficiency, low bandwidth due to the slow air-cooling speed and difficulty to achieve the precise control. Therefore, the development of new adaptive fuzzy controllers in order to improve the control system performance for processes with SMA actuators is motivated (Guerra et al., 2015; Alsayed et al., 2018; González et al., 2015; Nguyen et al., 2019; Shamloo et al., 2020; Matsumori et al., 2020).

Due to the need to compensate for the effects of Shape Memory Alloys process nonlinearities, the combination of fuzzy and adaptive control techniques can become important as they can ensure the CS performance improvement by the benefit from the specific advantages of each technique while keeping cost-effective implementations and therefore, the following control algorithms having fuzzy logic in their components are suitable to control the SMA actuators (Zhang et al., 2018; Senthilkumar et al., 2014; Quintanar-Guzmán et al., 2018; Dragoş et al., 2012).

Act 1.2 - Critical study of the possibilities to improve the existing control algorithms and to generate new adaptive fuzzy control algorithms *(In Romanian – Cercetarea posibilităţilor de îmbunătăţire a soluţiilor de reglare existente şi proiectarea de noi regulatoare fuzzy adaptive).* To accomplish this activity, the study of the existing fuzzy control algorithms and the possibility of the development of new adaptive fuzzy control algorithms were done.

The nonlinearities and the variable parameters of complex processes lead to the necessity of nonlinear controllers. Such representative intelligent controllers are type-1 and type-2 fuzzy ones, which are capable to provide high control system performances because it can model and minimize the effects of certain uncertainties (Castillo et al., 2011; Castillo et al., 2016). The concept of type-2 fuzzy sets was first suggested by Lotfi A. Zadeh in 1975, shortly after the concept of type-1 fuzzy sets. It was next treated systematically in (Karnik et al., 1999; Mendel, 2001) as an extended version that can overcome the limitations of type-1 fuzzy sets and type-1 fuzzy control in handling the parametric uncertainties in the model being capable of providing an extra degree of freedom to include different uncertainties like rule uncertainties, steady-state and dynamic load-type disturbances and noise.

As shown in (Bojan-Dragos et al., 2021), an overview focused on the past, present and future of type-2 fuzzy controllers, including their theoretical and practical implications, is conducted in (Mittal et al., 2020). Some recent applications of such controllers in automotive systems are briefly discussed as follows. The tracking performance improvement and the rejection of the external

disturbances of road specific to autonomous vehicles is carried out in (Taghavifar and Rakheja, 2019) using a fuzzy type-2 neural network controller with an exponential-like sliding surface. An interval type-2 fuzzy controller handles the uncertainties of driving conditions of hybrid electric autonomous vehicle in (Phan et al., 2020). A type-2 fuzzy controller is designed in (Dominik, 2016) to control the position of shape memory alloy wire actuators.

The shape change of membership functions makes the distinction between the type-1 and type-2 fuzzy systems. In type-1 ones, considering one input value, it is associated to just one membership function value in [0,1], unlike the type-2 ones, where the value of membership function form of a set of values in [0,1]. More exactly, in type-2 ones the membership functions are three-dimensional; the third dimension is the membership function value at each point on its two-dimensional domain; the name of this domain is the Footprint of Uncertainty (FOU).

In many applications, the desired performance indices (rise time, settling time, overshoot etc.) and the integral- or sum-type cost functions in properly defining optimization problems can be guarantee by the design and tuning of fuzzy control systems as shown in (Guerra et al., 2015; Precup et al., 2015). However, setting the optimization problems representative to the optimal tuning of fuzzy controllers is not simple especially in case of type-2 fuzzy ones because of the expressions of the cost functions and the risk to get trapped in local minima. Nature-inspired optimization algorithms as the popular swarm intelligence algorithms can be useful to minimize these cost functions as they exhibit reduced computational cost, transparency, and cost-effective design and implementation. Such algorithms include. Representative overviews on swarm intelligence algorithms in fuzzy control including type-2 fuzzy control are given in (Castillo et al., 2012; Castillo and Melin, 2014; Precup and David, 2019).

The elements of difficulty of the issue: (i) The stability analysis for some of the proposed approaches may be difficult to perform no matter what control algorithms are used (e.g. error linearization, frequency domain techniques, Lyapunov techniques). (ii) Environments where several constraints appear such as, for example, those imposed to the control signal and/or control signal rate, to the controlled output, etc. (iii) The extension of the approaches is expected to work for smooth nonlinear processes that can be well approximated with linear systems in the vicinity of nominal operating points. The potential impact to the scientific field may be significant because the proposed fuzzy control algorithms can be executable in a few minutes, the system stability analysis can be guaranteed using Lyapunov stability theory and the modern identification and control analysis, along with design methodologies, are based on various kinds of different representations that have different benefits and drawbacks in terms of identification and modeling effort and structure (Raja et al., 2018; Precup et al., 2014; Precup et al., 2003; Precup et al., 2006; Precup et al., 2020; Popov, 1973; Lendek et al., 2018). The potential impact of the project in the scientific, social, economic or cultural environment is straightforward as the new adaptive fuzzy control algorithms can lead to automatic tools for controller design and tuning in several control system structures with special focus of applicability to Shape Memory Alloys laboratory equipment: Shape Memory Alloys System, laboratory equipment with SMA, magnetic levitation system (Hedrea et al., 2017; Hedrea et al., 2019), two-rotor system, 3D crane system, ABS system.

The 2nd Stage of the project – The analysis, development, implementation and validation of the new control structures with adaptive fuzzy control algorithms by experiments on the laboratory equipment with SMA and on other laboratory equipment with SMA actuators and with the support of the external partners *(In Romanian – Analiza, proiectarea, implementarea și validarea noilor SRA cu regulatoarele fuzzy adaptive prin intermediul experimentelor pe echipamente de laborator în legătură cu SMA și alte echipamente de laborator cu elemente de execuție bazate pe SMA și prin intermediul partenerilor noștri externi).* – carried out during January-December 2021 has been fulfilled and is grouped in the form of the following activities:

Act 2.1 - The analysis of the actual theoretical framework with regard to the development of three adaptive fuzzy control algorithms by combination of fuzzy control and adaptive control, gain-scheduling control and sliding mode control to improve the control system performances *(In Romanian – Analiza cercetărilor actuale privind proiectarea a trei soluții de reglare fuzzy adaptivă prin combinarea reglării fuzzy cu reglarea adaptivă, reglarea gain-scheduling și reglarea în mod alunecător pentru a îmbunătății performanțele sistemelor de reglare automată).* To accomplish this activity, the analysis of the actual theoretical framework regarding the development of adaptive fuzzy control algorithms regarding controlling processes that include Shape Memory Alloys (SMA) actuators was considered.

The contribution of the team research members is important regarding the similar solutions studied in literature in the field since many current fuzzy controllers are of Mamdani type, while this

paper employs Takagi-Sugeno fuzzy controllers. In addition, it is difficult to control this kind of nonlinear process with SMA actuators and fuzzy control proves to be an initially relatively simple nonlinear control to cope with it. Therefore, in the followings details regarding the optimally tuning of the parameters of type-1 and type-2 fuzzy controllers for on Electromagnetic Actuated Clutch Systems with SMA actuators according to (Bojan-Dragos et al., 2021) are presented.

The parameter vector of the fuzzy controller (of type-1 and type-2) is the vector variable of the optimization problem which is solved by a GWO algorithm that targets the minimization of a cost function expressed as the sum of squared control errors

$$\boldsymbol{\rho}^{(J)*} = \arg\min_{\boldsymbol{\rho}^{(J)} \in D_{\rho}} J(\boldsymbol{\rho}^{(J)}) = \frac{1}{M}\sum_{k=1}^{N}[y_k^*(\boldsymbol{\rho}^{(J)}) - y_k(\boldsymbol{\rho}^{(J)})]^2 = \frac{1}{M}\sum_{k=1}^{N} e_k^2(\boldsymbol{\rho}^{(J)}), \tag{1}$$

where j denotes the controller type, $j \in \{\text{PI, TS-T1-FC, TS-T2-FC}\}$, the abbreviation TS-T1-FC is used for the adaptive Takagi-Sugeno type-1 fuzzy controller, the abbreviation TS-T2-FC is used for the adaptive Takagi-Sugeno type-2 fuzzy controller, $e_k(\boldsymbol{\rho}^{(J)}) = y_k^*(\boldsymbol{\rho}^{(J)}) - y_k(\boldsymbol{\rho}^{(J)})$ is the control error at k^{th} sampling interval, $y_k^*(\boldsymbol{\rho}^{(J)})$ is the reference input (the set-point), $y_k(\boldsymbol{\rho}^{(J)})$ is the controlled output, $\boldsymbol{\rho}^{(J)}$ is the controller parameter vector, D_{ρ} is the feasible domain of $\boldsymbol{\rho}^{(J)}$, and $\boldsymbol{\rho}^{(J)*}$ is the optimal controller parameter vector. The cost function $J(\boldsymbol{\rho}^{(J)})$ is a performance index that assesses the performance of the control system, and M in (1) s the length of the time horizon.

The initialization of the agents (i.e., wolves) is the first step GWO algorithms as pointed before in (Mirjalili et al., 2014) comprising the pack. Each agent of a total number of used N agents (i.e., grey wolves) will be modelled by its position vector $\mathbf{X}_i(\mu)$

$$\mathbf{X}_i(\mu) = [x_i^1(\mu) \quad \ldots \quad x_i^f(\mu) \quad \ldots \quad x_i^q(\mu)]^T, \; i = 1 \ldots N, \tag{2}$$

where $x_i^f(\mu)$ is the position of i^{th} agent in f^{th} dimension, $f = 1 \ldots q$, μ is the index of the current iteration, $\mu = 1 \ldots \mu_{\max}$, and $\mu_{\max}$ is the maximum number of iterations. Additional details on the GWO algorithm that is implemented in this paper and the associated vector operations are given in (Precup et al., 2016; Precup et al., 2017a; Precup et al., 2017b).

The GWO algorithm is mapped onto the optimization problems defined in (1) in terms of the following relationships:

$$\boldsymbol{\rho}^{(J)} = \mathbf{X}_i(\mu), \; i = 1 \ldots N, \tag{3}$$

$$\boldsymbol{\rho}^{(J)*} = \arg\min_{i=1\ldots N} J(\mathbf{X}_i(\mu_{\max})), \tag{4}$$

and the numbers of tuning parameters of the three controllers, with $j \in \{\text{PI, TS-T1-FC, TS-T2-FC}\}$, are q.

The process considered in this paper is an electromagnetic actuated clutch system with SMA actuators as part of electric drive clutches. Simplified nonlinear models can be accepted by neglecting the nonlinearities of the plant which are analysed in complete form and are included in the equation of the motion; the mechanical subsystem has the following dynamics

$$m\ddot{x} = F - c\dot{x} - kx, \tag{5}$$

and it is actuated by an electromagnetic subsystem with nonlinear characteristics. Its dynamic behaviour is characterized by (Di Cairano et al., 2007)

$$\dot{\lambda} = V - Ri, \quad \lambda = 2k_a i/(k_b + d - x), \quad F = k_a i^2/(k_b + d - x)^2 = \lambda^2/(4k_a). \tag{6}$$

The process parameters that appear in (5) and (6) have the numerical values adopted starting with (Di Cairano et al., 2007).

The presentation of the adaptive fuzzy controller structures and their design approach starts with outlining the theoretical support of TS-T1-FC. The design of the TS-T1-FC is based on the design of continuous-time PI controllers, where good recommendations are given in (Åström and Hägglund, 1995). The PI controller is discretized using Tustin's method with the sampling period T_s to obtain the equations of the discrete-time PI controller in its incremental form widely used in quasi-continuous digital control (Precup and David, 2019)

$$\Delta u_k = \gamma(\eta K_P \Delta e_k + K_I e_k), \quad K_P = k_C(1 - T_s/(2T_o)), \; K_I = k_C T_s / T_C, \tag{7}$$

where: e_k – the control error, Δe_k – the increment of control error, Δu_k – the increment of control signal, K_P and K_I – the parameters of the digital PI controller, and the additional parameters γ and

η allow the improvement of the input-output map of the fuzzy controller in order to modify and adjust the control system performance.

The first equation in (7) indicates that the parameters γ and η are not needed and their presence increases artificially the number of tuning parameters of TS-T1-FC. They can be dropped out and included in K_P and K_I, and thus reduce the number of tuning parameters with two and the search space as well. However, these two parameters are kept in the design to highlight that the fuzzy controller design starts here with the design of the linear PI controller, and the knowledge from that is next transferred to the fuzzy controller structure and design. This motivation is also used as far as TS-T2-FC is concerned. In addition, the input variables of both TS-T1-FC and TS-T2-FC are also scheduling variables.

Linguistic terms (LTs) with uniform distribution membership functions, whose optimal parameters will be obtained in the next section according to the GWO algorithm, are employed. The inference engine uses the MIN and MAX operators and the weighted average method for defuzzification is included in TS-T1-FC structure. In TS-T2-FC the rules remain the same as in TS-T1-FC, but the antecedents and the consequents are described by type 2 fuzzy sets. The rest of sub-systems operate in TS-T2-FC in the same manner as in TS-T1-FC.

Fig. 1 illustrates the block diagram of an adaptive TS-2-FC structure. It includes five sub-systems: fuzzifier, rule base, inference engine, type-reducer and defuzzifier. The inputs are the control error and its increment, and a single output is used, in TS-2-FC considered in paper and built around a linear PI controller, namely the increment of control signal.

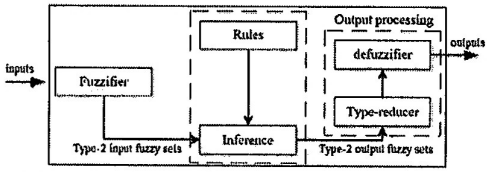

Fig. 1. Structure of type-2 fuzzy controller (Phan et al., 2020).

But the main difference between TS-T1-FC and TS-T2-FC is that the second one employs type 2 fuzzy sets, and this it includes an extra process which is known as the essential type-reducer sub-system. Karnik and Mendel (1998) designed a popular type-reducer, which calculates the centroids of type 2 sets and of the type-reduced set. While using the usual centroid type-reduced the firing output set is generated from by each fuzzy rule.

The GWO-based tuning approach that ensures the optimal tuning of TS-T1-FC and TS-T2-FC consists of three steps:

Step A. A linear tuning method is applied to initially obtain the parameters of the linear PI controllers, then T_s is fixated and the discrete-time PI controllers in (7) are achieved.

Step B. The dynamic regime involved in the evaluation of the cost function in (1) is defined. This includes the setting of the time horizon which includes all transients of the fuzzy control system until the cost function will obtain the value of steady-state. All constraints imposed to the elements of $\boldsymbol{\rho}^{(J)}$ are included in the feasible domain D_{ρ}.

Step C. The GWO algorithms are used to calculate the optimal parameter vector $\boldsymbol{\rho}^{(J)*}$.

Act 2.2 - The development of stability for the proposed control systems with the new adaptive fuzzy control algorithms using different stability methods *(In Romanian – Asigurarea stabilității SRA cu noile regulatoare fuzzy adaptive utilizând diverse metode de stabilitate).* To accomplish this activity, the analysis of stability for the control systems with adaptive fuzzy control algorithms was done using different stability methods.

The stability analysis of the proposed CS is presented as follows. This stability analysis is also carried out in (Bojan-Dragos et al., 2019; Hedrea et al., 2019; Precup et al., 1999; Precup et al., 2020). Similar fuzzy controllers are used in (Bojan-Dragos et al., 2019; Hedrea et al., 2019) but the nonlinear process controlled is different. For performing the stability analysis, the dynamics of the fuzzy controller (FC) is transferred to the process, and this leads to the extended controlled process (EP), illustrated in Fig. 2 (a) (Precup and Preitl, 1997). For the sake of simplicity the stability analysis is presented below in an unified manner for both control structures, where $\mathbf{w}_k = \begin{bmatrix} w_k & \Delta w_k \end{bmatrix}^T$ with w_k the reference input, $\Delta w_k = w_k - w_{k-1}$ the increment of reference input, $\mathbf{e}_k = \begin{bmatrix} e_k & \Delta e_k \end{bmatrix}^T$, with: e_k the control error, Δe_k the increment of control error, $\mathbf{y}_k = \begin{bmatrix} y_k & \Delta y_k \end{bmatrix}^T$, with: y_k the controlled output,

$\Delta y_k=y_k-y_{k-1}$ the increment of controlled output, $\mathbf{u}_k=\left[\Delta u_k \quad \Delta u_{fk}\right]^T$, where u_{fk} represents the fictitious control signal, Δu_{fk} stands for the fictitious increment of control signal, $\Delta u_{fk}=u_{fk}-u_{fk-1}$ (Bojan-Dragos et al., 2019; Hedrea et al., 2019; Precup and Preitl, 1997; Precup and Preitl, 2003).

The FC block is characterized by the nonlinear input-output static map **F**

$$\mathbf{F}: R^2 \to R^2, \mathbf{F}(\mathbf{e}_k)=\left[f(\mathbf{e}_k) \quad 0\right]^T, \tag{8}$$

where f ($f: R^2 \to R$) is the input-output static map of the nonlinear block without dynamics inserted for steady-state and dynamic CS performance improvement.

The state-space mathematical models are next expressed as:

$$\begin{aligned} \mathbf{x}_{k+1} &= \mathbf{A}\ \mathbf{x}_k + \mathbf{B}\mathbf{u}_k, \\ \mathbf{y}_k &= \mathbf{C}\mathbf{x}_k, \end{aligned} \tag{9}$$

by inserting additional state variables, which result in the augmented state vectors $\mathbf{x}_k=\left[\mathbf{x}_k \quad x_{uk} \quad x_{yk}\right]^T$, due to the presence of the additional linear dynamics transferred from the fuzzy PI controller structures, (Bojan-Dragos et al., 2019; Hedrea et al., 2019; Precup and Preitl, 1997; Precup and Preitl, 2003).

Therefore, the resulting state-space matrices are

$$\mathbf{A}=\begin{bmatrix} \mathbf{A} & \mathbf{b} & \mathbf{0} \\ \mathbf{0}^T & 1 & 0 \\ \mathbf{c}^T & 0 & 0 \end{bmatrix}, \mathbf{B}=\begin{bmatrix} \mathbf{b} & 1 \\ 1 & 1 \\ 0 & 1 \end{bmatrix}, \mathbf{C}=\begin{bmatrix} \mathbf{c}^T & 0 & 0 \\ \mathbf{c}^T & 0 & -1 \end{bmatrix}, \ \mathbf{A}\in\Re^{n\times n}, \mathbf{B}\in\Re^{n\times 2}, \mathbf{C}\in\Re^{2\times n}, \tag{10}$$

where n is the order of the mathematical models.

The structure presented in Fig. 2 (b) is used in the stability analysis of the nonlinear CS, where the NL block represents a static nonlinearity due to the nonlinear part without dynamics of the FC block. The connections between the variables of the CS structures in Figs. 2 (a) and (b) are

$$\mathbf{v}_k=-\mathbf{u}_k=-\mathbf{F}(\mathbf{e}_k), \mathbf{y}_k=-\mathbf{e}_k, \tag{11}$$

where the second component of **F** is always zero in order to neglect the effect of fictitious control signal.

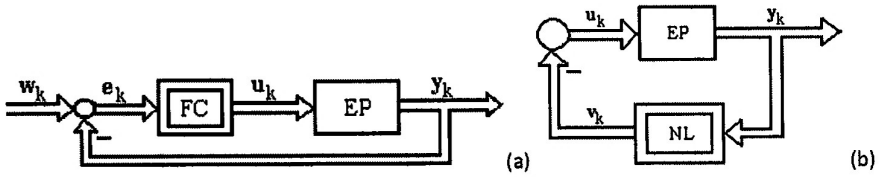

Fig. 2. Modified structure of fuzzy CS (a); Structure of nonlinear control system involved in stability analysis (b).

By taking into account the relation (11), the second equations in (9) become:

$$\begin{aligned} \mathbf{e}_k &= -\mathbf{C}\mathbf{u}_k, \mathbf{x}_k = \mathbf{C}^b\mathbf{e}_k, \end{aligned} \tag{12}$$

where the matrix $\mathbf{C}^b$, ($\mathbf{C}^b\in\Re^{n\times 2}$), can be computed relatively easily as function of **C**.

The stability analysis theorem is (Precup and Preitl, 1997; Precup and Preitl, 2003):

Theorem 1. The nonlinear system whose structure is given in Fig. 2 (b) and whose mathematical model is presented (9) is globally asymptotically stable if the conditions I and II are fulfilled by the matrices **P**, **L** and **V**:

I. $(\mathbf{A})^T\mathbf{P}\cdot\mathbf{A}=-\mathbf{L}\mathbf{L}^T$, $\mathbf{C}-(\mathbf{B})^T\mathbf{P}\cdot\mathbf{A}=\mathbf{V}^T\mathbf{L}^T$, $-(\mathbf{B})^T\mathbf{P}\cdot\mathbf{B}=\mathbf{V}^T\mathbf{V}$. (13)

II. By introducing the matrices **M** ($\mathbf{M}\in\Re^{2\times 2}$), **N** ($\mathbf{N}\in\Re^{2\times 2}$) and **R** ($\mathbf{R}\in\Re^{2\times 2}$) defined as follows:

$$\mathbf{M}=(\mathbf{C}^b)^T(\mathbf{L}\mathbf{L}^T-\mathbf{P})\mathbf{C}^b, \quad \mathbf{R}=\mathbf{V}^T\mathbf{V}, \quad \mathbf{N}=(\mathbf{C}^b)^T[\mathbf{L}\mathbf{V}-(\mathbf{A})^T\mathbf{P}\mathbf{B}^a-2(\mathbf{C})^T, \tag{14}$$

the next inequality holds for any value of control error e_k:

$$f(\mathbf{e}_k)\mathbf{n}^T\mathbf{e}_k+(\mathbf{e}_k)^T\mathbf{M}\,\mathbf{e}_k\geq 0, \tag{15}$$

where the vector $\mathbf{e}_k$ is defined in (11) and **n** represents the first column of **N**.

Proof. The first condition (I) represents the first equation from the Kalman-Szegö lemma; therefore, it is fulfilled (Landau, 1979).

In order to fulfil the second condition (II), the Popov inequality (15), which ensures the global asymptotic stability of the nonlinear CS for any positive constant β_0, is expressed:

$$S(k_1)=\sum_{k=0}^{k_1}(\mathbf{v}_k)^T\mathbf{y}_k\geq-\beta_0^2\ \ \forall k_1\in N^*. \tag{16}$$

Considering (11), the Popov sum $S(k_1)$ becomes:

$$S(k_1)=-\sum_{k=0}^{k_1}(\mathbf{u}_k)^T\mathbf{y}_k\ \ \forall k_1\in N^*. \tag{17}$$

By substituting in (17) the expression of $\mathbf{x}_{k+1}$ and $\mathbf{y}_k$ from (9), followed by adding and subtracting the term $(\mathbf{x}_{k+1})^T\mathbf{P}\cdot\mathbf{x}_{k+1}$ and using the properties of matrix transposition the Popov sum $S(k_1)$ becomes:

$$S(k_1)=-\sum_{k=0}^{k_1}\{-(\mathbf{x}_k)^T(\mathbf{A})^T\mathbf{P}\cdot\mathbf{A}\mathbf{x}_k-(\mathbf{x}_k)^T[(\mathbf{A})^T(\mathbf{P}++\mathbf{P}^T)\mathbf{B}+ \tag{18}$$

$$(\mathbf{C})^T]\mathbf{u}_k-(\mathbf{u}_k)^T(\mathbf{B})^T\mathbf{P}\cdot\mathbf{B}\cdot\mathbf{u}_k+(\mathbf{x}_{k+1})^T\mathbf{P}\cdot\mathbf{x}_{k+1}]\}\ \ \forall k_1\in N^*.$$

By replacing the expressions of $(\mathbf{A})^T\mathbf{P}\cdot\mathbf{A}$, $(\mathbf{A})^T\mathbf{P}^T\cdot\mathbf{B}$ and $(\mathbf{B})^T\mathbf{P}\cdot\mathbf{B}$ from the condition (I) and by expressing $\mathbf{x}_k$ from (12) and using the condition (II), another form of the Popov sum $S(k_1)$ is obtained:

$$S(k_1)=-\sum_{k=0}^{k_1}(\mathbf{x}_{k+1})^T\mathbf{P}\cdot\mathbf{x}_{k+1}+\sum_{k=0}^{k_1}[(\mathbf{e}_k)^T\mathbf{M}\cdot\mathbf{e}_k+(\mathbf{e}_k)^T\mathbf{N}\cdot\mathbf{u}_k+(\mathbf{u}_k)^T\mathbf{R}\cdot\mathbf{u}_k]\ \ \forall k_1\in N^*. \tag{19}$$

Using the expression of $\mathbf{u}_k$ in (11), (19) becomes:

$$S(k_1)=-\sum_{k=0}^{k_1}(\mathbf{x}_{k+1})^T\mathbf{P}\cdot\mathbf{x}_{k+1}+\sum_{k=0}^{k_1}[(\mathbf{e}_k)^T\mathbf{M}\cdot\mathbf{e}_k+(\mathbf{e}_k)^T\mathbf{N}\cdot\mathbf{F}(\mathbf{e}_k)+\mathbf{F}^T(\mathbf{e}_k)\mathbf{R}\cdot\mathbf{F}(\mathbf{e}_k)]\ \ \forall k_1\in N^*. \tag{20}$$

Finally, the expression of the sum $S(k_1)$ is obtained by using **F** from (8) and the positive element r_{11} of matrix **R**:

$$S(k_1)=-\sum_{k=0}^{k_1}[(\mathbf{x}_{k+1})^T\mathbf{P}\cdot\mathbf{x}_{k+1}+r_{11}f^2(\mathbf{e}_k)]+\sum_{k=0}^{k_1}[(\mathbf{e}_k)^T\mathbf{M}\cdot\mathbf{e}_k+f(\mathbf{e}_k)\mathbf{n}^T\cdot\mathbf{e}_k]\ \ \forall k_1\in N^*. \tag{21}$$

Both sums in (21) are positive and therefore the sum $S(k_1)$ is also positive, which means that the condition (II) guarantees the fulfilment of the Popov inequality (16). In conclusion, the fuzzy CS globally asymptotically stable, therefore Theorem 1 is proved.

For $n > 2$, only the matrix **P** from the first condition (I) is significant for the fuzzy CS stability analysis because the matrices **M**, **N** and **R** from the second condition (II) can be expressed as functions of **P**.

$$\mathbf{M}=-(\mathbf{C}^b)^T(\mathbf{A})^T\mathbf{P}\cdot\mathbf{A}\mathbf{C}^b,\ \mathbf{R}=-(\mathbf{B})^T\mathbf{P}\cdot\mathbf{B},\ \ \mathbf{N}=-(\mathbf{C}^b)^T[(\mathbf{A})^T(\mathbf{P}+\mathbf{P}^T)\mathbf{B}+(\mathbf{C})^T]. \tag{22}$$

The stable design of the controllers is non-homogenous. The reduction of process parametric sensitivity can be treated to alleviate this shortcoming or model–free control can be employed, but the latter is difficult to be related to stability because of the lack of parametric models in controller tuning. A general stable design approach to state-feedback control is given in (Pozna and Precup, 2018), and a stable design approach to fuzzy control systems is given (Precup et al., 2014); both approaches avoid the LMIs, however they depend on the process models.

Act 2.3 - The implementations, testing and validation of the new control structures with adaptive fuzzy control algorithms by simulation or by experiments on laboratory equipment with SMA and on other laboratory equipment with SMA actuators. *(In Romanian – Implementarea, testarea și validarea noilor SRA cu regulatoare fuzzy adaptive prin simulare sau prin experimente pe echipamente de laborator în legătură cu SMA si pe alte echipamente de laborator cu elemente de execuție bazate pe SMA).* To accomplish this activity, the developed adaptive fuzzy control algorithms regarding controlling processes that include Shape Memory Alloys (SMA) actuators were implemented, tested and validated on simulated laboratory equipment with SMA.

The sampling period has been set in step A to $T_s=0.01\,\mathrm{s}$ in order to implement quasi-continuous digital controllers. The feasible domains of $\boldsymbol{\rho}^{(J)}$ in terms of the three optimization problems used as search spaces were set appropriately. The dimensions of the feasible domains (and also search spaces) are q=2 for the PI controller, q=12 for TS-T1-FC and q=7 for TS-T2-FC. The dynamic regime in step B is characterized by zero initial conditions and the 2 mm step modification

of the reference input on a time horizon of 1.2 s. The values of the parameters of the GWO algorithms that solves in step C the optimization problems in (1) were set as follows in order to ensure an acceptable trade-off to convergence speed and accuracy: the number of the agents N = 500 and the maximum number of iterations $\mu_{\max} = 20$.

The particular expression of the parameter vector of the PI controller is

$$\boldsymbol{\rho}^{(1)} = [k_c \quad T_c]^T, \tag{23}$$

where T stands for matrix transposition, the particular expressions of the parameter vector of TS-T1-FC is

$$\boldsymbol{\rho}^{(2)} = [B_e \quad B_{\Delta e} \quad \gamma^1 \quad \eta^1 \quad \gamma^2 \quad \eta^2 \quad \gamma^3 \quad \eta^3 \quad \gamma^4 \quad \eta^4 \quad \gamma^5 \quad \eta^5]^T, \tag{24}$$

where B_e and $B_{\Delta e}$ are the parameters of the membership functions of the input LTs, and the parameters $\gamma^i, i = 1...5$, and $\eta^i, i = 1...5$, introduce extra nonlinearities to adjust the performance of the control systems. The particular expressions of the parameter vector of TS-T2-FC described above is

$$\boldsymbol{\rho}^{(3)} = [L_l \quad L_{sf1} \quad L_{sf2} \quad L_{sf3} \quad L_{sf4} \quad L_{sf5} \quad L_{sf6}]^T, \tag{25}$$

where L_l is the lower membership function lag value and L_{scfi}, i = 1...6, is the lower membership function scaling factor for the membership function of both input variables.

The application of a GWO algorithm leads to the following optimal tuning parameter vectors of the PI controller which ensure the system stability because the stability conditions are checked to validate the next solution candidate:

$$\boldsymbol{\rho}^{(1)*} = [74.7688 \quad 0.0898]^T. \tag{26}$$

The fuzzification sub-system in TS-T1-FC makes use of the LTs attributed to the input and also scheduling variables e_k and Δe_k, defined in the following two cases, 11 and 12.

Case 11. Three LTs with trapezoidal and triangular membership functions for both input variables are used. The following nine rules with the parameters $K_P = 6.34$ and $K_I = 0.38$ of the PI controllers placed in the rule consequents leads to the complete rule base of TS-T1-FC:

$$\begin{aligned}
&\mathbf{R1}: \text{IF } e_k \text{ IS N AND } \Delta e_k \text{ IS N THEN } \Delta u_k = \gamma^5[\eta^5 K_P \Delta e_k + K_I e_k], \mathbf{R2}: \text{IF } e_k \text{ IS N AND } \Delta e_k \text{ IS ZE THEN } \Delta u_k = \gamma^4[\eta^4 K_P \Delta e_k + K_I e_k],\\
&\mathbf{R3}: \text{IF } e_k \text{ IS N AND } \Delta e_k \text{ IS P THEN } \Delta u_k = \gamma^3[\eta^3 K_P \Delta e_k + K_I e_k], \mathbf{R4}: \text{IF } e_k \text{ IS ZE AND } \Delta e_k \text{ IS N THEN } \Delta u_k = \gamma^2[\eta^2 K_P \Delta e_k + K_I e_k],\\
&\mathbf{R5}: \text{IF } e_k \text{ IS ZE AND } \Delta e_k \text{ IS ZE THEN } \Delta u_k = \gamma^1[\eta^1 K_P \Delta e_k + K_I e_k], \mathbf{R6}: \text{IF } e_k \text{ IS ZE AND } \Delta e_k \text{ IS P THEN } \Delta u_k = \gamma^2[\eta^2 K_P \Delta e_k + K_I e_k],\\
&\mathbf{R7}: \text{IF } e_k \text{ IS P AND } \Delta e_k \text{ IS N THEN } \Delta u_k = \gamma^3[\eta^3 K_P \Delta e_k + K_I e_k], \mathbf{R8}: \text{IF } e_k \text{ IS P AND } \Delta e_k \text{ IS N THEN } \Delta u_k = \gamma^4[\eta^4 K_P \Delta e_k + K_I e_k],\\
&\mathbf{R9}: \text{IF } e_k \text{ IS P AND } \Delta e_k \text{ IS P THEN } \Delta u_k = \gamma^5[\eta^5 K_P \Delta e_k + K_I e e_k].
\end{aligned} \tag{27}$$

The GWO algorithm applied in the terms given above conducts to the following optimal tuning parameter vector of TS-T1-FC which ensures the system stability:

$$\boldsymbol{\rho}^{(2)*} = [13.8252 \; 19.6579 \; 5.7156 \; 0.2461 \; 5.9587 \; 0.1515 \; 5.736 \; 0.087 \; 3.4285 \; 0.2577 \; 3.6969 \; 0.0558]^T. \tag{28}$$

Case 12. Three LTs with a spline-based Z-shaped membership function, a Gaussian membership function and a spline-based S-shaped membership function for both input variables are used. The same complete rule base given in (27) was used. The GWO-based solving of (3) leads to the following optimal tuning parameter vector of TS-T1-FC which ensures the system stability:

$$\boldsymbol{\rho}^{(2)*} = [16.6814 \; 12.9926 \; 1.4641 \; 0.5128 \; 1.1202 \; 0.0883 \; 0.9555 \; 0.0894 \; 0.8646 \; 0.2625 \; 1.0427 \; 0.1069]^T. \tag{29}$$

Two cases were also considered for the input variables in the fuzzification sub-system of TS-T2-FC, 21 and 22, with the results described as follows.

Case 21. The membership function distribution for particular inputs of the TS-T2-FC is trapezoidal and triangular (Fig. 3), with the value of FOU optimally tuned by a GWO algorithm. The enhanced Karnik-Mendel method was implemented in the type-reducer sub-system.

The GWO algorithm conducts to the following optimal tuning parameter vector of TS-T2-FC which ensures the system stability:

$$\boldsymbol{\rho}^{(3)*} = [0.1 \quad 0.1 \quad 0.1 \quad 0.1 \quad 0.1 \quad 0.1 \quad 0.1]^T. \tag{30}$$

Case 22. A spline-based Z-shaped membership function, a Gaussian membership function and a spline-based S-shaped membership function (illustrated in Fig. 3) were used, with the value of

FOU obtained on the basis of a GWO algorithm. The GWO algorithm leads to the following optimal tuning parameter vector of TS-T2-FC which ensures the system stability:

$$\rho^{(3)*} = [0.0251\ 0.051\ 0.8\ 0.051\ 0.051\ 0.8\ 0.051]^T. \quad (31)$$

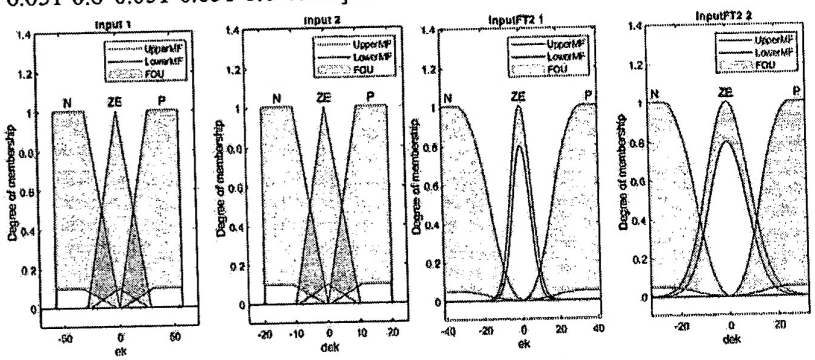

Fig. 3. Input membership functions in cases 21 and 22.

To highlight the difference between the control systems with the developed adaptive fuzzy control algorithms some simulation scenarios were done. Therefore, the proposed adaptive fuzzy control algorithms were tested and validated on simulated laboratory equipment with SMA actuators. The simulation scenarios are characterized by the application of a set of step-type modifications of the reference input.

The simulation results illustrated in Fig. 4 (a) give the response of the control system with TS-T1-FC obtained in the cases 11 and 12 illustrating the measured position in time. The simulation results illustrated in Fig. 4 (b) give the response of the control system with TS-T2-FC obtained in the cases 21 and 22, also illustrating the measured position in time. The simulation results presented in Fig. 5 (a) show the response of the control system with TS-T1-FC obtained in the cases 11 and with TS-T2-FC obtained in the case 21 illustrating the measured position in time, which is similar to the other figures considered here. Finally, the simulation results presented in Fig. 5 (b) show the response of the control system with TS-T1-FC obtained in the cases 12 and with TS-T2-FC obtained in the case 22, illustrating the measured position in time.

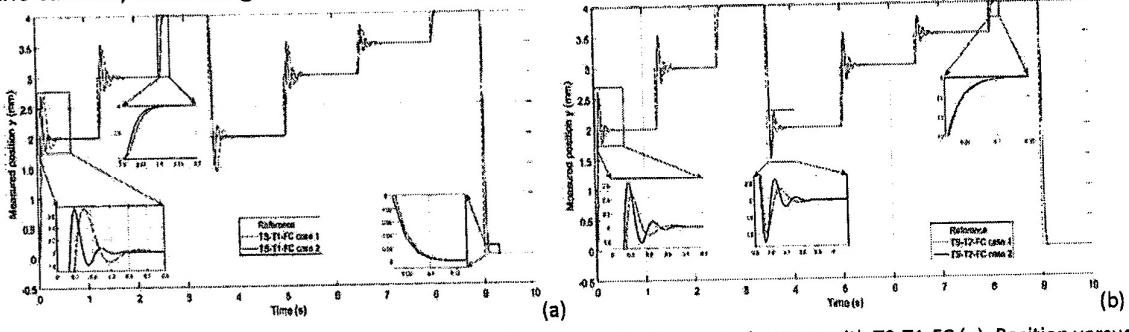

Fig. 4. Position versus time obtained in the cases 11 and 12 concerning the control system with TS-T1-FC (a); Position versus time obtained in the cases 21 and 22 concerning the control system with TS-T2-FC (b).

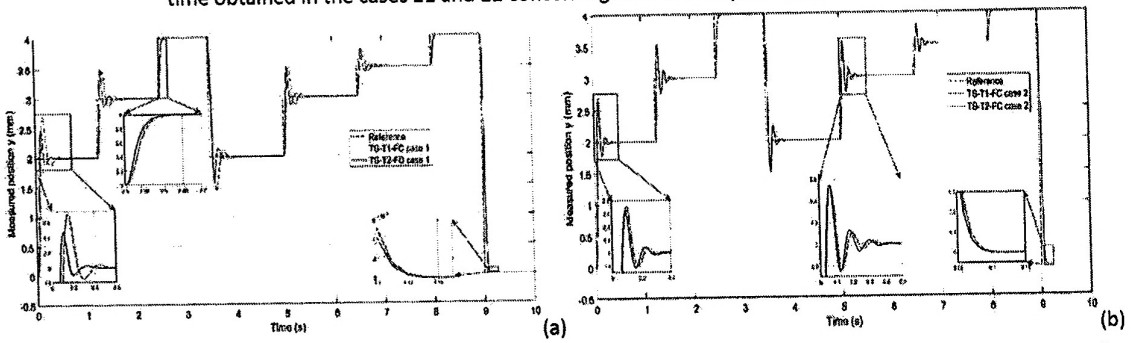

Fig. 5. Position versus time obtained In *the case 11 concern*ing the control system with TS-T1-FC and the case 21 concerning the control system with TS-T2-FC (a); Position *versus time obtained in* the case 12 concerning the control system with TS-T1-FC and the case 22 concerning the control system with TS-T2-FC (b).

The measured value of the cost functions are $J(\rho^{(\text{TS-T1-FC})}) = 0.1055$ in the case 11,

$J(\rho^{(TS\text{-}T2\text{-}FC)}) = 0.0888$ in the case 21, $J(\rho^{(TS\text{-}T1\text{-}FC)}) = 0.0875$ in the case 21 and $J(\rho^{(TS\text{-}T2\text{-}FC)}) = 0.0853$ in the case 22. The presented results show very good control system expressed in terms of small cost function values. Therefore, the proposed adaptive fuzzy controllers are validated by simulation results. The good performances are obtained by the adaptive fuzzy control system with TS-T2-FC.

Act 2.4 - The validation of the new control structures with nonlinear controllers with the support of the external partners (Continental Automotive Timişoara, Airbus Helicopters Romania – through direct connections timely consolidated, Ontario Center of Excellence – through our Ottawa team partner) *(In Romanian – Validarea noilor SRA cu regulatoare neliniare prin intermediul partenerilor din mediul privat (Continental Automotive Timişoara, Airbus Helicopters Romania prin relaţii directe consolidate în timp, Ontario Center of Excellence prin intermediul partenerul nostru din Ottawa, Canada).* To accomplish this activity, the developed adaptive fuzzy control algorithms were implemented, tested, and validated on laboratory equipment with SMA from the external partners.

Due to the pandemic period, no experiments could be done in the industry. Therefore, we intend after the pandemic period and after we will be allowed to travel for long periods, these validations will be followed: the developed adaptive fuzzy control algorithms presented in (Bojan-Dragos et al., 2021) on electromagnetic actuated clutch systems with SMA actuators laboratory equipment from the Gheorghe Asachi" Technical University of Iasi, Romania through our external partner Prof. Corneliu Lazar and his team, the iterative feedback tuning algorithm proposed in (Roman et al., 2021) on laboratory equipment from Bremen University, Germany, through our team partner Prof. Axel Gräser and his team and the tensor product-based model transformation technique proposed in (Hedrea et al., 2021) on a servo system laboratory equipment of University of Debrecen, Hungary, in cooperation with Prof. Péter Korondi and of Szechenyi Istvan University, Gyor, Hungary, in cooperation with Prof. Péter Baranyi and his team. All control solutions proposed in (Precup et al., 2021a; Precup et al., 2021b) and (Roman et al., 2021) which include sliding mode and fuzzy control and slime mould algorithm-based tuning of cost-effective fuzzy controllers, developed for servo processes with SMA actuators will also be tested and validated on laboratory equipment of Ontario Centers of Excellence – through our Ottawa team partner and his team.

The 3rd Stage of the project – The testing, verification and validation of the new adaptive fuzzy control algorithms by experiments on the laboratory equipment with SMA and with the support of the external partners *(In Romanian – Testarea, verificarea şi validarea noilor regulatoare fuzzy adaptive prin intermediul experimentelor pe echipamente de laborator în legătură cu SMA şi prin intermediul partenerilor noştri externi)* – carried out during January-September 2022 has been fulfilled and is grouped in the form of the following activities:

Act 3.1 - The development of stability for the proposed control systems with the new adaptive fuzzy control algorithms using different stability methods *(In Romanian – Asigurarea stabilităţii SRA cu noile regulatoare fuzzy adaptive utilizând diverse metode de stabilitate).* To accomplish this activity, the analysis of stability for the control systems with adaptive fuzzy control algorithms was done using different stability methods. Details are presented in the study in section B.

As shown in (Bojan-Dragos et al., 2022b), the analysis of the state-of-the-art of control theory and applications related to Shape Memory Alloy (SMA) actuators presented in (Soother et al., 2020; Bojan-Dragos, 2021; Keshtkar et al., 2021) shows that they are in continuous progress, and they can ensure very good control system performance. This is enabled because of their specific feature, namely they can keep a distorted shape until warmth is applied to regain their original shape (Kim et al., 2013) and can have the capability to high strain recovery and withstanding the higher load and high damping and supporting major reversible changes in mechanical and physical properties (Lagoudas, 2008). The above features and the need to validate the control system structures for SMA actuators as controlled processes in both simulation and experimental results are a reason of their wide variety of applications as biomedical engineering (Andrianesis and Tzes, 2014), robotics (Yang et al., 2019), industry, vibration control systems (Alsayed et al., 2018; Suhel et al., 2018; Matsumori et al., 2020), aeronautics and aviation (Dominik, 2016). SMA testing equipment was designed in both simple cases and complicated ones to model them (Precup et al., 2021) and to design nonlinear robust controllers for position and tracking control (Dominik, 2016; Mituletu et al., 2019).

The mathematical models of SMA actuators are nonlinear as their work in two phases, the heating and the cooling transition, which give rise to hysteresis (Precup et al., 2021). Therefore, in some cases for modelling the SMA behaviour several system identification approaches implemented in Matlab's System Identification Toolbox were used in (Dominik, 2016) to describe the system model as a linear one with uncertainties and next control them with robust stability methods. Representative nonlinear models of SMA actuators are the fuzzy ones, which are relatively easily understandable and may embed the human expert's knowledge in dealing with the processes. The

evolving fuzzy (or rule-based) controllers derived in (Precup et al., 2020; Precup et al., 2021) employ evolving Takagi-Sugeno-Kang (TSK) fuzzy models, which are characterised by continuous online rule base learning, and which are developed in terms of evolving the model structures and parameters by means of online identification algorithm (Blazic et al., 2014; Ferdaus et al., 2020). The nonlinearities of SMA actuators may justify the nonlinear type-1 and type-2 fuzzy controllers capable to ensure high control system performance by modelling and minimisation of the effects of certain uncertainties (Castillo et al., 2016; Dominik, 2016; Bojan-Dragos et al., 2021; Castillo et al., 2011). A complete overview of type-2 fuzzy controllers is presented in (Mittal et al., 2020). The main difference between the type-1 and the interval type-2 fuzzy systems is caused by the membership function shapes, more exactly in type-1 ones one membership function value in [0,1] is associated to one input value and in type-2 ones the membership functions are three-dimensional.

Since it is difficult to cope with the nonlinearities of SMA wire actuators, the use of nonlinear controllers is a serious option. The motivation for the proposed controllers developed in the followings is their relatively simple design and implementation making them attractive in industrial applications with these actuators.

The optimisation problems involved in the optimal tuning of both SMA models and controllers target the minimisation of the cost functions $J(\boldsymbol{\rho}^{(J)})$ in the form (1) detailed in the 2nd stage of the project where $\boldsymbol{\rho}^{(J)*}$ is the optimal parameter vector of the process model, i.e., SMA wire actuator, or the controller, $\boldsymbol{\rho}^{(J)}$ is the vector of the parameters of the process model or controller, D_{ρ} is the feasible domain of $\boldsymbol{\rho}^{(J)}$, j indicates the type of process model and controller, the superscript $j \in$ {PT2-Td, PD1T3-Td, PID-C, FT1-C, FT2-C, SM-C, STSM-C}, PT2-Td indicates a second-order low pass filter with delay model, PD1T3-Td indicates a proportional-derivative with a third order low pass filter and delay model, FT1-C indicates a Takagi-Sugeno-Kang (TSK) type-1 fuzzy controller, FT2-C indicates a TSK interval type-2 fuzzy controller, SM-C indicates a sliding mode controller, STSM-C indicates a super-twisting sliding mode controller, M is the length of the time horizon, $y_k^*(\boldsymbol{\rho}^{(J)})$ is the output of the real-world SMA wire actuator or the reference input, i.e., the desired SMA output, $y_k(\boldsymbol{\rho}^{(J)})$ is the controlled output of the process model, i.e., the position of SMA wire actuator, $e_k(\boldsymbol{\rho}^{(J)})$ is the modelling error or the control error, and k is the index of the current sampling interval.

The following GWO algorithm steps are used to obtain the optimally tuned parameters of PT2-Td model, PD1T3-Td model, FT1-C, FT2-C, SM-C and STSM-C are:

Step A. The dynamic regime implicated in the evaluation of the cost function in (1) – namely, (i) setting the time horizon which includes all transients of the fuzzy control system until the controlled output reaches its steady-state value, (ii) setting the variations of the input signals applied to the control system, and (iii) setting the initial conditions – is defined. The feasible domain D_{ρ} includes constraints imposed to the elements of $\boldsymbol{\rho}^{(J)}$.

Step B. The optimal parameter vector $\boldsymbol{\rho}^{(J)*}$ is calculated by a GWO algorithm.

To ensure good control system performances and to not to get stuck in a local minimum the following values of the parameters of the GWO algorithms applied in step B of the tuning approach were set: the number of the agents $N = 100$ and the maximum number of iterations $\mu_{max} = 100$.

The nonlinear process model used in this paper is one of the evolved TSK fuzzy models of SMA wire actuators derived by Precup et al. (2021), which is validated against the experimental data reported by Dominik (2016). The output of the SMA wire actuator considered in (Dominik, 2016), and viewed as controlled processes, is the position, and the input is the current signal which supplies the actuator, i.e., it flows through the wire. The output will next be used as a controlled output and the input as a control signal (or control input) in the position control systems.

Starting with this TSK fuzzy model, two simple linear dynamic system models, namely a second-order low pass filter with delay (PT2-Td) model and a proportional-derivative with a third order low pass filter and delay (PD1T3-Td) model are identified, with the following transfer functions (t.f.s), P_{PT2-Td} and $P_{PD1T3-Td}$:

$$P_a(s) = [k_a / ((1 + T_{1-a}s)(1 + T_{2-a}s))]e^{-T_{d-a}s}, \tag{32}$$

$$P_b(s) = [(k_b(1 + sT_{z-b})) / ((1 + T_{1-b}s)(1 + T_{2-b}s)(1 + sT_{3-b}))]e^{-T_{d-b}s}, \tag{33}$$

where a=PT2-Td and b=PD1T3-Td are the model types, k_a and k_b are the process gains, T_{1-a}, T_{2-a}, T_{1-b}, T_{2-b} and T_{3-b} are the time constants, T_{z-b} is the derivative time constant, T_{d-a} and T_{d-b} are the time delays.

The parameter vector of PT2-Td is

$$\boldsymbol{\rho}^{(1)} = [k_a \quad T_{1-a} \quad T_{2-a} \quad T_{d-a}]^T, \tag{34}$$

where T indicates matrix transposition, and q = 4. The dynamic regime involved in step A of the tuning approach is the training regime described in (Precup et al., 2021), characterised by a time horizon of 5 s (for a sampling period of 0.01 s) and zero initial conditions.

The optimal parameter vector of PT2-Td obtained by the application of the GWO algorithm in step B of the tuning approach is

$$\boldsymbol{\rho}^{(1)*} = [8.0049 \quad 0.4 \quad 0.1 \quad 0.0005]^T. \tag{35}$$

The parameter vector of PD1T3-Td is

$$\boldsymbol{\rho}^{(2)} = [k_b \quad T_{z-b} \quad T_{1-b} \quad T_{2-b} \quad T_{3-b} \quad T_{d-b}]^T, \tag{36}$$

where q = 6. Using the same dynamic regime as before, the GWO algorithm applied in step B of the tuning approach leads to the optimal parameter vector of PD1T3-Td:

$$\boldsymbol{\rho}^{(2)*} = [8.0566 \; 0.4298 \; 0.5284 \; 0.3096 \; 0.0018 \; 0.06]^T. \tag{37}$$

The first comparison is carried out between one of the evolved TSK fuzzy models of SMA wire actuators in (Precup et al., 2021), which ensures the best experimental data fitting but pays the cost of rather many parameters, the two linear dynamic system models derived in this paper, and the linear dynamic system models derived in (Dominik, 2016), with the t.f.

$$G(s) = 167.3/(s^2 + 15.19s + 18.98). \tag{38}$$

Fig. 6 illustrates the responses of these four models.

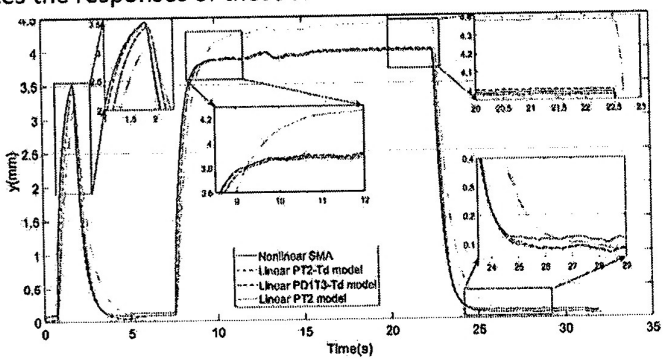

Fig. 6. Position versus time for nonlinear (i.e., TSK fuzzy) and linear models of SMA wire actuators.

The measured values of the cost function in this first model comparison are $J(\boldsymbol{\rho}^{(1)}) = 0.0288$ in the case of PT2-Td with the parameters in (35) and $J(\boldsymbol{\rho}^{(2)}) = 0.0041$ in the case of PD1T3-Td with the parameters in (37).

To control the position of the SMA wire actuators, PID-Cs are considered with the t.f. $C_{PID}(s)$

$$C_{PID}(s) = k_p + k_i/s + k_d s, \tag{39}$$

where k_p is the controller proportional gain, k_i is the controller integral gain, and k_d is the controller derivative gain.

The parameter vector of PID-C is

$$\boldsymbol{\rho}^{(3)} = [k_p \quad k_i \quad k_d]^T, \tag{40}$$

where q = 3. The dynamic regime involved in step A of the tuning approach employs a time horizon of 35 s (for a sampling period of 0.01 s), zero initial conditions, and six step-type modifications of the reference input, i.e., the set-point or the desired SMA position.

The optimal parameter vector of PID-C obtained by the application of the GWO algorithm in step B of the tuning approach is

$$\boldsymbol{\rho}^{(3)*} = [1.3165 \quad 3.5089 \quad 0.0037]^T. \tag{41}$$

Matlab's PID Tuner was used in (Dominik, 2016) to tune the parameters of PID-C based on the created model leading to k_p=0.20, k_i=0.47 and k_d=0. However, after additional manual tuning in the experimental testing conducted on the real-world SMA wire actuator, the PID-C parameter values considered by Dominik (2016) are: k_p=0.17, k_i=0.40 and k_d= 0.01.

The next control solution designed to control the position of the SMA wire actuators is the sliding mode control solution with the structure given in Fig. 7, where the tuning parameters specific to SM-C are $T_i > 0$, $\alpha > 0$ and $c > 0$.

The control law, which has a variable structure and is specific to SM-C, is expressed as

$$u(t) = \psi(t)u_e(t) + (1/T_i)\int_0^t \psi(t)u_e(\tau)d\tau, \tag{42}$$

where T_i is the integral time constant and the nonlinear switching and product-based terms are

$$\psi(t) = \alpha \operatorname{sgn}(\sigma(t)e(t)),\ u_e(t) = \psi(t)e(t). \tag{43}$$

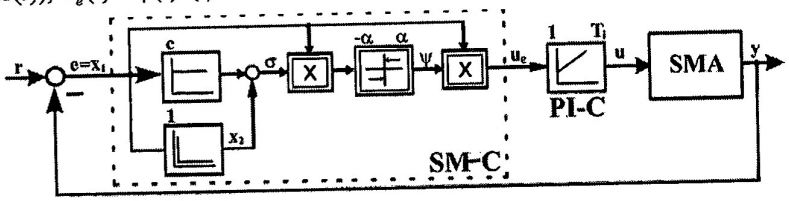

Fig. 7. SM-C structure.

In order to improve the control system performance, the parameters of the PI quasi relay sliding-mode controller are tuned using three types of methods detailed in the followings. Also, details regarding the accomplishment of the ***Activity 3.1*** which include the stability analysis of the control system with the two proposed sliding mode controllers, are presented in the following paragraphs.

In the ***first method*** the tuning parameters of the PI quasi relay sliding-mode controller are obtained in the following design steps:

Step 1. Basically, the parameter T_i =0.5284 can be determined in terms of the pole-zero cancelation regarding the t.f. of the plant expressed in (33).

Step 2. In order to design the sliding mode control law, the switching variable $\sigma(t)$ is defined as

$$\sigma(t) = c\,x_1(t) + x_2(t), \tag{44}$$

where the tuning parameter $c = \text{const} > 0$ prescribes the desired behaviour of the control system on the sliding manifold (line), so is chosen taking into account the impose performances: $c = 6 < a_2$, where the constant parameter a_2 together with the constant parameters a_1 and b, and the disturbance term f are the parameters in the Ackerman's form of the state-space equations of the closed-loop system

$$\begin{aligned} \dot{x}_1(t) &= x_2(t), \\ \dot{x}_2(t) &= -a_1 x_1(t) - a_2\, x_2(t) + b\, u_{1x}(t) + f(t), \end{aligned} \tag{45}$$

The expressions of the parameters are:

$$a_1 = 1/[T_{1\_b} * (T_{2\_b} + T_{3\_b})],\ a_2 = 2*(T_{1\_b} + T_{2\_b} + T_{3\_b})/[T_{1\_b} * (T_{2\_b} + T_{3\_b})]$$
$$b = -0.1 * k_b/[T_{1\_b} * (T_{2\_b} + T_{3\_b})],\ f = 1/[T_{1\_b} * (T_{2\_b} + T_{3\_b})] \tag{46}$$

The numerical values of these parameters and disturbance term are $a_1 = 6.0774,\ a_2 = 10.2076,\ b = -4.8963,\ f = 10.1055$.

Step 3. Using the following Lyapunov function $V(t) = 0.5\sigma^2(t)$, the sliding mode reaching and existence condition:

$$\sigma(t)\,\dot{\sigma}(t) < 0. \tag{48}$$

is determined based on the **global asymptotical stability condition** of **Lyapunov's stability theory**, $\dot{V}(t) < 0$.

From (44), the derivative $\dot{\sigma}(t)$ is obtained as

$$\dot{\sigma}(t) = c\,\dot{x}_1(t) + \dot{x}_2(t) = -a_1 x_1(t) + (c - a_2)\,x_2(t) + b u_{1x}(t) + f. \tag{49}$$

Replacing $x_2(t)=\sigma(t)-cx_1(t)$ from (44) in (49) and next (48), the existence condition (48) becomes

$$\sigma(t)\dot{\sigma}(t)=-\sigma(t)[(a_1+c^2-a_2c)x_1(t)-bu_{1x}(t)-f]+(c-a_2)\sigma^2(t)<0. \quad (50)$$

The term $(c-a_2)\sigma^2(t)$ in (50) is always negative due to the fact that $c<a_2$, therefore a sufficient condition to fulfill (48) is

$$\sigma(t)[(a_1+c^2-a_2c)x_1(t)-bu_{1x}(t)-f]>0. \quad (51)$$

The substitution of the control signal using (42) and (43) in (51) leads to

$$\sigma(t)[(a_1+c^2-a_2c)x_1(t)-b\alpha x_1(t)\mathrm{sgn}(\sigma(t)x_1(t))+(b\alpha/T_i)\int_0^t x_1(\tau)\mathrm{sgn}(\sigma(\tau)x_1(\tau))d\tau-f]>0. \quad (52)$$

Depending on the sign of $\sigma(t)$, two cases are next considered:

Case 1. $\sigma(t)>0$. Therefore (52) results in

$$(a_1+c^2-a_2c)x_1(t)-b\alpha x_1(t)\mathrm{sgn}(\sigma(t)x_1(t))+(b\alpha/T_i)\int_0^t x_1(\tau)\mathrm{sgn}(\sigma(\tau)x_1(\tau))d\tau-f(t)>0. \quad (53)$$

The sufficient condition (53) is transformed into

$$b\alpha<[(a_1+c^2-a_2c)x_1(t)-f(t)]/[|x_1(t)|+(1/T_i)\int_0^t|x_1(\tau)|d\tau]. \quad (54)$$

Case 2. $\sigma(t)<0$. Therefore (52) results in

$$(a_1+c^2-a_2c)x_1(t)-b\alpha x_1(t)\mathrm{sgn}(\sigma(t)x_1(t))+(b\alpha/T_i)\int_0^t x_1(\tau)\mathrm{sgn}(\sigma(\tau)x_1(\tau))d\tau-f(t)<0. \quad (55)$$

The sufficient condition (55) is transformed into

$$b\alpha<-[(a_1+c^2-a_2c)x_1(t)-f(t)]/[|x_1(t)|+(1/T_i)\int_0^t|x_1(\tau)|d\tau]. \quad (56)$$

The following sufficient condition can guarantee the sliding mode reaching and existence condition and it is obtained based on these two cases reflected in (54) and (56):

$$b\alpha<-[|(a_1+c^2-a_2c)x_1(t)-f(t)|]/[|x_1(t)|+(1/T_i)\int_0^t|x_1(\tau)|d\tau]. \quad (57)$$

In the ***second method*** the parameters obtained in the first method at the step 1 and 2, T_i, a_1, a_2, b, f and $c>0$, are optimally tuned using the GWO algorithm. The parameter vector of SM-C is

$$\boldsymbol{\rho}^{(4)}=[T_i \quad a_1 \quad a_2 \quad b \quad f \quad c]^T, \quad (58)$$

The GWO algorithm applied in step B of the tuning approach leads to the optimal parameter vector of PI-SM-C:

$$\boldsymbol{\rho}^{(4)*}=[0.402 \quad 3.6107 \quad 9.5413 \quad -5.7573 \quad 3.9156 \quad 4.7303]^T. \quad (59)$$

In the ***third method*** the parameters $T_i>0$, $\alpha>0$ and $c>0$ of the PI quasi relay sliding-mode controller are optimally tuned using the GWO algorithm. Therefore, the parameter vector of SM-C is

$$\boldsymbol{\rho}^{(5)}=[T_r \quad \alpha \quad c]^T, \quad (60)$$

The GWO algorithm applied in step B of the tuning approach leads to the optimal parameter vector of SM-C:

$$\boldsymbol{\rho}^{(5)*}=[0.3765 \quad 1.3979 \quad 1.0325]^T. \quad (61)$$

In the context of higher order SMC theory, the super-twisting sliding mode algorithms (STSM-C) are second-order schemes, also named "2-sliding controllers" useful to control the outputs of second order systems, or to avoid chattering for first order systems (Lascu et al., 2013; Levant, 1993; Levant, 2003; Levant, 2005; Levant, 2007). STSM-C have the distinct feature that their trajectories in the phase plane display a spiral (twisted) motion pattern while converging to the origin asymptotically or in finite time (Levant, 2005). The main idea of STSM-C is to apply the switching action to the higher order derivatives of the control quantity, u, instead of its first derivative like in conventional SMC. In this way the sliding movement occurs on a set of higher order derivatives of the

sliding surface, in which vicinity the control converges to the equivalent control and thus the chattering can be avoided. The convergence can be asymptotical or with finite time, depending on the switching scheme used. The stability of such a controller can be proved for all second order sliding controllers, as shown in (Lascu et al., 2013; Levant, 2005).

The structure of STSM-C is given in Fig. 8, where the tuning parameters specific to STSM-C are the same like in the SM-C, $T_i > 0$, $\alpha > 0$ and $c > 0$. The control law, which has a variable structure and is specific to STSM-C, is expressed as

$$u(t) = \psi(t)\sqrt{u_e(t)} + (1/T_i)\int_0^t \psi(t)u_e(\tau)d\tau, \tag{62}$$

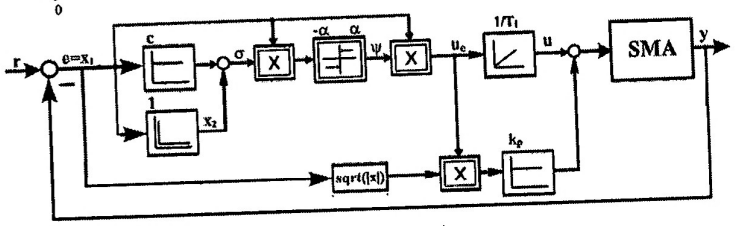

Fig. 8. STSM-C structure.

The parameters of the STSM-C are also tuned using three types of methods like in SM-C case and are detailed in the followings.

In the ***first method*** the tuning parameters of the STSM-C are the same as in the SM-C case so they are obtained in same manner as in the SM-C case and the numerical values of these parameters and disturbance term are $a_1 = 6.0774$, $a_2 = 10.2076$, $b = -4.8963$, $f = 10.1055$.

In the ***second method*** the parameters of STSM-C, T_i, a_1, a_2, b, f and $c > 0$, are optimally tuned using the GWO algorithm. The parameter vector of SM-C is

$$\boldsymbol{\rho}^{(6)} = [T_i \quad a_1 \quad a_2 \quad b \quad f \quad c]^T, \tag{63}$$

The GWO algorithm applied in step B of the tuning approach leads to the optimal parameter vector of STSM-C:

$$\boldsymbol{\rho}^{(6)*} = [0.4175 \quad 3.3914 \quad 9.5463 \quad -5.7573 \quad 3.8429 \quad 4.5514]^T. \tag{64}$$

In the ***third method*** the parameters of STSM-C, $T_i > 0$, $\alpha > 0$ and $c > 0$, are optimally tuned using the GWO algorithm. Therefore, the parameter vector of STSM-C is

$$\boldsymbol{\rho}^{(7)} = [T_r \quad \alpha \quad c]^T, \tag{65}$$

The GWO algorithm applied in step B of the tuning approach leads to the optimal parameter vector of STSM-C:

$$\boldsymbol{\rho}^{(7)*} = [0.3806 \quad 1.4347 \quad 1.0412]^T. \tag{66}$$

The second comparison is carried out between the control systems with SM-C and STSM-C designed above. The control system (CS) responses are illustrated in Figs. 9-11 as follows: CS with SM-C with the parameters obtained using the first designed method and CS with SM-C with the parameters obtained using the second designed method are illustrated in Fig. 9 (a); CS with STSM-C with the parameters obtained using the first designed method and CS with STSM-C with the parameters obtained using the second designed method are illustrated in Fig. 9 (b); CS with SM-C and CS with STSM-C with the parameters obtained using the first designed method are illustrated in Fig. 10 (a); CS with SM-C and CS with STSM-C with the parameters obtained using the second designed method are illustrated in Fig. 10 (b); CS with SM-C and STSM-C with the parameters obtained using the first designed method and CS with SM-C and STSM-C with the parameters obtained using the second designed method are illustrated in Fig. 11 (a); CS with SM-C and CS with STSM-C with the parameters obtained using the third designed method are illustrated in Fig. 11 (b). The dynamic regime in this comparison, which sets the simulation scenario, is that used in the optimal tuning of the controller parameters described above, namely it employs a time horizon of 35 s (for a sampling period of 0.01 s), zero initial conditions, and six step-type modifications of the reference input.

The measured values of the cost function in this first model comparison are: $J(\boldsymbol{\rho}^{(4)}) = 0.0145$ in the case of SM-C with the parameters in (59), $J(\boldsymbol{\rho}^{(6)}) = 0.0136$ in the case of STSM-C with the parameters in (64), $J(\boldsymbol{\rho}^{(5)}) = 0.0103$ in the case of SM-C with the parameters in (61), $J(\boldsymbol{\rho}^{(7)}) = 0.0091$ in the case of STSM-C with the parameters in (66).

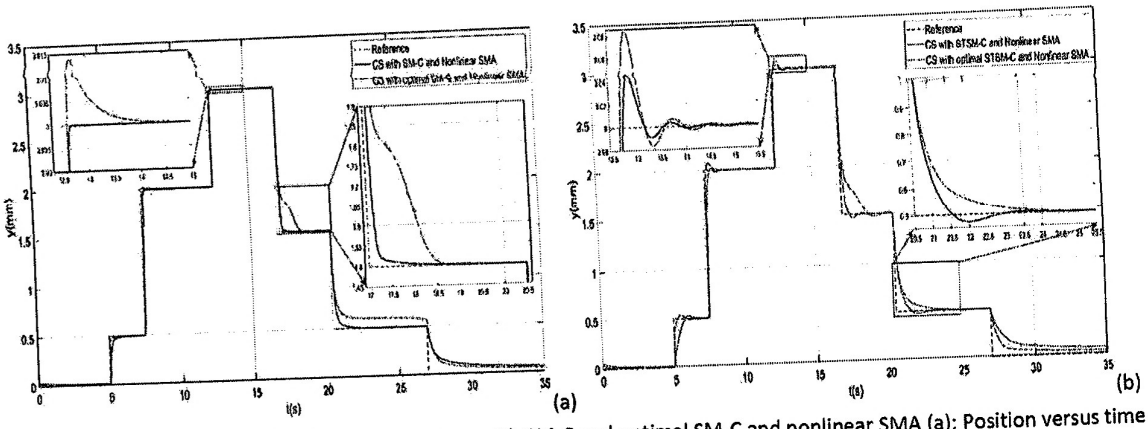

Fig. 9. Position versus time for the control systems with SM-C and optimal SM-C and nonlinear SMA (a); Position versus time for the control systems with STSM-C and optimal STSM-C and nonlinear SMA (b).

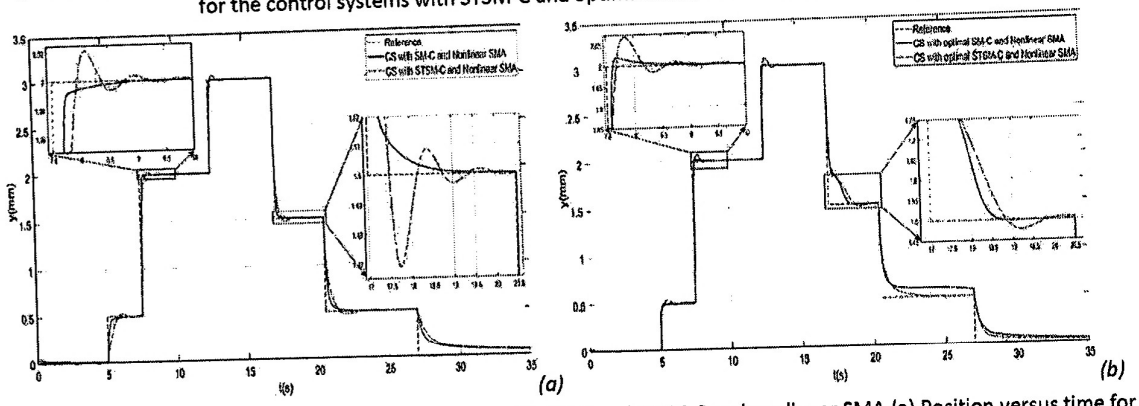

Fig. 10. Position versus time for the control systems with SM-C and STSM-C and nonlinear SMA (a) Position versus time for the control systems with optimal SM-C and optimal STSM-C and nonlinear SMA (b).

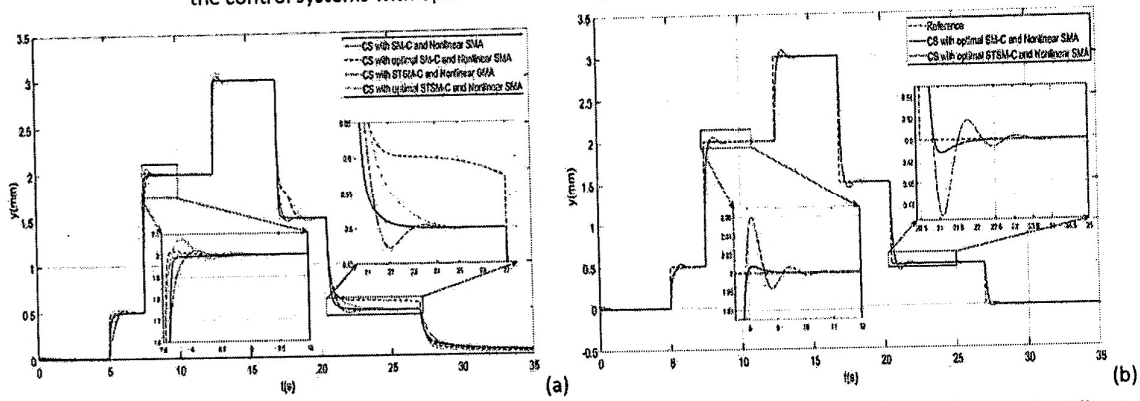

Fig. 11. Position versus time for the control systems with SM-C, optimal SM-C, STSM-C and optimal STSM-C and nonlinear SMA (a); Position versus time for the control systems with optimal SM-C and optimal STSM-C with the parameters tuned using the third method (b).

The control law taken into consideration in the design of the FT1-C is based on the incremental form of a discrete-time PI controller (Åström and Hägglund, 1995):

$$\Delta u_k = K_P \Delta e_k + K_I e_k, \tag{67}$$

where e_k is the control error, Δe_k is the control error increment, Δu_k is the control signal increment, K_P and K_I are the parameters of the linear PI controllers, which will be tuned in the next section using GWO algorithm.

The FT2-C structure includes the fuzzifier sub-systems, the rule base sub-systems, the inference engine sub-systems, the type-reducer sub-systems and the defuzzifier sub-systems and it is illustrated in Fig. 12 (a) (Phan et al., 2021). In the context of (67), two inputs, which are also scheduling variables, are used in the FT1-C, namely e_k and Δe_k, and a single output is involved, Δu_k, in both FTC-1 and FTC-2.

Fig. 12 (b) illustrates that interval type 2 fuzzy sets require the inclusion of an extra type-reducer sub-system with respect to FT1-C structure. One such popular sub-system was designed by Karnik and Mendel (1998) to calculate the centroids of type 2 sets and of the type-reduced set. While using the usual centroid type-reduced each fuzzy rule generates the firing output set. The rest of sub-systems operate in FT2-C in the same manner as in FT1-C.

The fuzzification sub-system in FT1-C and FT2-C makes use of three linguistic terms (LTs) with trapezoidal membership functions and triangular membership functions for the input variables e_k and Δe_k, which are scheduling variables as well. The parameters of the input membership functions of FTC-2 are illustrated in Fig. 12 (b).

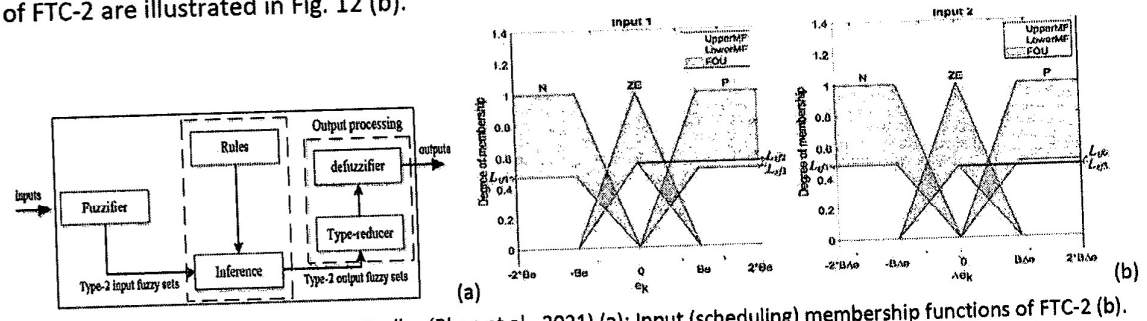

Fig. 12. Structure of type-2 fuzzy controller (Phan et al., 2021) (a); Input (scheduling) membership functions of FTC-2 (b).

The specific TSK-type rule base of FT1-C and FTC-2 contains linear PI controllers in its consequents, and the following nine rules represent the complete rule base of FT1-C and FTC-2 in order to ensure the best performance indices:

$$\begin{aligned}
&\mathbf{R1}: \text{IF } e_k \text{ IS N AND } \Delta e_k \text{ IS N THEN } \Delta u_k = K_P^5 \Delta e_k + K_I^5 e_k, \mathbf{R2}: \text{IF } e_k \text{ IS N AND } \Delta e_k \text{ IS ZE THEN } \Delta u_k = K_P^4 \Delta e_k + K_I^4 e_k,\\
&\mathbf{R3}: \text{IF } e_k \text{ IS N AND } \Delta e_k \text{ IS P THEN } \Delta u_k = K_P^3 \Delta e_k + K_I^3 e_k, \mathbf{R4}: \text{IF } e_k \text{ IS ZE AND } \Delta e_k \text{ IS N THEN } \Delta u_k = K_P^2 \Delta e_k + K_I^2 e_k,\\
&\mathbf{R5}: \text{IF } e_k \text{ IS ZE AND } \Delta e_k \text{ IS ZE THEN } \Delta u_k = K_P^1 \Delta e_k + K_I^1 e_k, \mathbf{R6}: \text{IF } e_k \text{ IS ZE AND } \Delta e_k \text{ IS P THEN } \Delta u_k = K_P^2 \Delta e_k + K_I^2 e_k,\\
&\mathbf{R7}: \text{IF } e_k \text{ IS P AND } \Delta e_k \text{ IS N THEN } \Delta u_k = K_P^3 \Delta e_k + K_I^3 e_k, \mathbf{R8}: \text{IF } e_k \text{ IS P AND } \Delta e_k \text{ IS N THEN } \Delta u_k = K_P^4 \Delta e_k + K_I^4 e_k,\\
&\mathbf{R9}: \text{IF } e_k \text{ IS P AND } \Delta e_k \text{ IS P THEN } \Delta u_k = K_P^5 \Delta e_k + K_I^5 e_k.
\end{aligned} \tag{68}$$

The optimal parameters of the LTs with uniformly distributed membership functions will be optimally tuned in the next section by a GWO algorithm. In the inference engine the MIN and MAX operators are used, and the weighted average method is used for defuzzification. These above-described structures of the two fuzzy controllers and (68) indicate that both FTC-1 and FTC-2 exhibit behaviours of nonlinear bumpless interpolators between five separate discrete-time PI controllers placed in the rule consequents.

The parameter vector of FT1-C is

$$\boldsymbol{\rho}^{(8)} = [B_e \quad B_{\Delta e} \quad K_P^1 \quad K_I^1 \quad K_P^2 \quad K_I^2 \quad K_P^3 \quad K_I^3 \quad K_P^4 \quad K_I^4 \quad K_P^5 \quad K_I^5]^T, \tag{69}$$

where B_e and $B_{\Delta e}$ are the parameters of the membership functions of the LTs of the input (scheduling) variables illustrated in Fig. 12 (b), and q = 12. Using the dynamic regime of the control system described above in the context of PID-C, the GWO algorithm applied in step B of the tuning approach leads to the optimal parameter vector of FT1-C:

$$\boldsymbol{\rho}^{(8)*} = [472.9471 \ 7.0611 \ 0.109 \ 1.4241 \ 0.0804 \ 2.0235 \ 0.0405 \ 1.1487 \ 0.0549 \ 1.4856 \ 0.0533 \ 0.9002]^T. \tag{70}$$

The parameter vector of FT2-C is

$$\begin{aligned}
\boldsymbol{\rho}^{(9)} = [&B_e \quad B_{\Delta e} \quad K_P^1 \quad K_I^1 \quad K_P^2 \quad K_I^2 \quad K_P^3 \quad K_I^3 \quad K_P^4 \quad K_I^4 \quad K_P^5 \quad K_I^5\\
&L_{sf1} \quad L_{sf2} \quad L_{sf3} \quad L_{sf4} \quad L_{sf5} \quad L_{sf6}]^T,
\end{aligned} \tag{71}$$

where L_{sfi}, $i = 1...6$, are the scaling factors of the lower membership functions illustrated in Fig. 12 (b), and q = 18 in the context of (71). Using the same dynamic regime of the control system as that used for PID-C and FT1-C, the GWO algorithm applied in step B of the tuning approach leads to the optimal parameter vector of FT2-C:

$$\begin{aligned}
\boldsymbol{\rho}^{(9)*} = [&720.49 \ 8.8211 \ 0.0501 \ 1.7346 \ 0.1262 \ 1.8009 \ 0.1354 \ 1.7509 \ 0.132 \ 1.4851 \ 0.0971 \ 1.6279\\
&0.4681 \ 0.5519 \ 0.5058 \ 0.4853 \ 0.4688 \ 0.497]^T.
\end{aligned} \tag{72}$$

The third comparison is carried out between the control systems with PID-C designed above and PID-C designed by Dominik (2016). The control system responses are illustrated in Fig. 13 (a). The dynamic regime in this comparison, which sets the simulation scenario, is that used in the optimal tuning of the controller parameters described above, namely it employs a time horizon of 35 s (for a sampling period of 0.01 s), zero initial conditions, and six step-type modifications of the reference input. The third comparison is carried out between the control systems with FT1-C and FT2-C in the same simulation scenario as above. The control system responses are presented in Fig. 13 (b).

The measured values of the cost function in these linear and nonlinear controller comparisons are: $J(\boldsymbol{\rho}^{(3)}) = 0.0048$ in the case of the control system with PID-C with the parameters in (41), $J(\boldsymbol{\rho}^{(4)}) = 0.0046$ in the case of the control system with FT1-C with the parameters in (70), $J(\boldsymbol{\rho}^{(5)}) = 0.0040$ in the case of the control system with FT2-C with the parameters in (72).

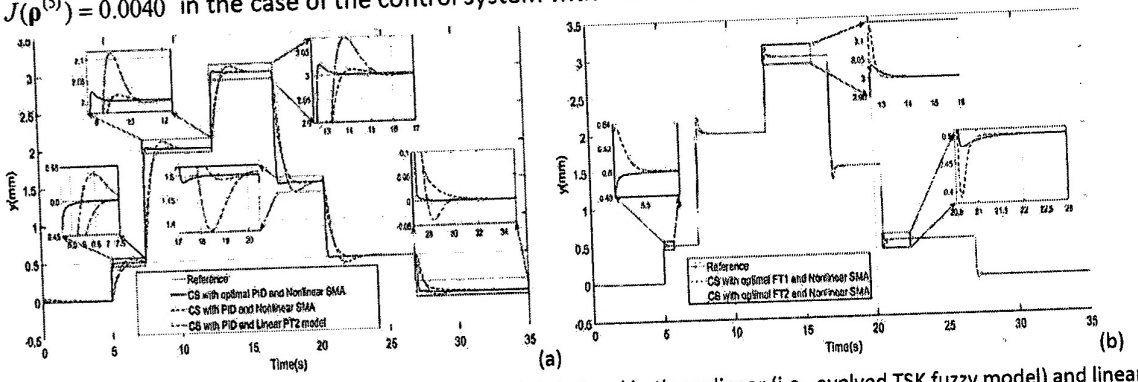

Fig. 13. Position *versus time for the* control systems with PID-C and both nonlinear (i.e., evolved TSK fuzzy model) and linear models of SMA wire actuator (CS – control system) (a); Position versus time for the control systems with FT1-C and FT2-C and nonlinear model (i.e., evolved TSK fuzzy model) of SMA wire actuators (CS – control system) (b).

These results show very good control system performance expressed in terms of small cost function values. In addition, the last two comparisons and the validation of the proposed controllers by simulation results indicate that the best performance is obtained by the fuzzy control system with FT2-C. Since the type-1 and type-2 fuzzy controllers developed by Dominik (2016) do not ensure good performance as reference input and control error are employed as input and scheduling variables, this paper does not include the comparison with those fuzzy controllers.

In the following paragraphs, details regarding the accomplishment of the ***Activity 3.1*** are presented. For performing the stability analysis of the control system with the two proposed adaptive fuzzy controller, the dynamics of the FT1-C and FT2-C are transferred to the process, and this leads to the extended controlled process (EP), illustrated in Fig. 14 (a) (Precup and Preitl, 1997). For the sake of simplicity the stability analysis is presented below in an unified manner for both control structures, where $\mathbf{w}_k = \begin{bmatrix} w_k & \Delta w_k \end{bmatrix}^T$ with w_k the reference input, $\Delta w_k = w_k - w_{k-1}$ the increment of reference input, $\mathbf{e}_k = \begin{bmatrix} e_k & \Delta e_k \end{bmatrix}^T$, with: e_k the control error, Δe_k the increment of control error, $\mathbf{y}_k = \begin{bmatrix} y_k & \Delta y_k \end{bmatrix}^T$, with: y_k the controlled output, $\Delta y_k = y_k - y_{k-1}$ the increment of controlled output, $\mathbf{u}_k = \begin{bmatrix} \Delta u_k & \Delta u_{fk} \end{bmatrix}^T$, where u_{fk} represents the fictitious control signal, Δu_{fk} stands for the fictitious increment of control signal, $\Delta u_{fk} = u_{fk} - u_{fk-1}$ (Bojan-Dragos et al., 2019; Hedrea et al., 2019; Precup and Preitl, 1997; Precup and Preitl, 2003).

The FT1-C / FT2-C block is characterized by the nonlinear input-output static map **F**

$$\mathbf{F}: R^2 \to R^2, \mathbf{F}(\mathbf{e}_k) = \begin{bmatrix} f(\mathbf{e}_k) & 0 \end{bmatrix}^T, \tag{73}$$

where f ($f: R^2 \to R$) is the input-output static map of the nonlinear block without dynamics inserted for steady-state and dynamic CS performance improvement.

The state-space mathematical models are next expressed as:

$$\begin{aligned} \mathbf{x}_{k+1} &= \mathbf{A}\,\mathbf{x}_k + \mathbf{B}\mathbf{u}_k, \\ \mathbf{y}_k &= \mathbf{C}\mathbf{x}_k, \end{aligned} \tag{74}$$

by inserting additional state variables, which result in the augmented state vectors $\mathbf{x}_k = \begin{bmatrix} \mathbf{x}_k & x_{uk} & x_{yk} \end{bmatrix}^T$, due to the presence of the additional linear dynamics transferred from the sliding mode controller structures, (Bojan-Dragos et al., 2019; Hedrea et al., 2019; Precup and Preitl, 1997; Precup and Preitl, 2003).

Therefore, the resulting state-space matrices are

$$\mathbf{A}=\begin{bmatrix}\mathbf{A} & \mathbf{b} & \mathbf{0}\\ \mathbf{0}^T & 1 & 0\\ \mathbf{c}^T & 0 & 0\end{bmatrix},\mathbf{B}=\begin{bmatrix}\mathbf{b} & \mathbf{1}\\ 1 & 1\\ 0 & 1\end{bmatrix},\mathbf{C}=\begin{bmatrix}\mathbf{c}^T & 0 & 0\\ \mathbf{c}^T & 0 & -1\end{bmatrix},\mathbf{A}\in\Re^{nxn},\mathbf{B}\in\Re^{nx2},\mathbf{C}\in\Re^{2xn}, \tag{75}$$

where n is the order of the mathematical models.

The structure presented in Fig. 14 (b) is used in the stability analysis of the nonlinear CS, where the NL block represents a static nonlinearity due to the nonlinear part without dynamics of the FC block.

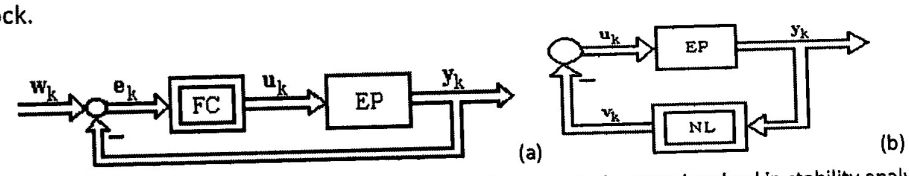

Fig. 14. Modified structure of fuzzy CS (a); Structure of nonlinear control system involved in stability analysis (b).

The connections between the variables of the CS structures in Fig. 14 (a) and (b) are

$$\mathbf{v}_k=-\mathbf{u}_k=-\mathbf{F}(\mathbf{e}_k),\mathbf{y}_k=-\mathbf{e}_k, \tag{76}$$

where the second component of **F** is always zero in order to neglect the effect of fictitious control signal.

By taking into account the relation (76), the second equations in (74) become:

$$\mathbf{e}_k=-\mathbf{C}\mathbf{u}_k,\mathbf{x}_k=\mathbf{C}^b\mathbf{e}_k, \tag{77}$$

where the matrix $\mathbf{C}^b$, ($\mathbf{C}^b\in\Re^{nx2}$), can be computed relatively easily as function of **C**.

The stability analysis theorem is detailed the followings (Precup and Preitl, 1997; Precup and Preitl, 2003).

Theorem 1. The nonlinear system whose structure is given in Fig. 14 (b) and whose mathematical model is presented (74) is globally asymptotically stable if the conditions I and II are fulfilled by the matrices **P**, **L** and **V**:

$$\text{I.}\quad (\mathbf{A})^T\mathbf{P}\cdot\mathbf{A}=-\mathbf{L}\mathbf{L}^T,\ \ \mathbf{C}-(\mathbf{B})^T\mathbf{P}\cdot\mathbf{A}=\mathbf{V}^T\mathbf{L}^T,\ \ -(\mathbf{B})^T\mathbf{P}\cdot\mathbf{B}=\mathbf{V}^T\mathbf{V}. \tag{78}$$

II. By introducing the matrices **M** ($\mathbf{M}\in\Re^{2x2}$), **N** ($\mathbf{N}\in\Re^{2x2}$) and **R** ($\mathbf{R}\in\Re^{2x2}$) defined as follows:

$$\mathbf{M}=(\mathbf{C}^b)^T(\mathbf{L}\mathbf{L}^T-\mathbf{P})\mathbf{C}^b,\ \ \mathbf{R}=\mathbf{V}^T\mathbf{V},\ \ \mathbf{N}=(\mathbf{C}^b)^T[\mathbf{L}\mathbf{V}-(\mathbf{A})^T\mathbf{P}\mathbf{B}^n-2(\mathbf{C})^T, \tag{79}$$

the next inequality holds for any value of control error e_k:

$$f(\mathbf{e}_k)\mathbf{n}^T\mathbf{e}_k+(\mathbf{e}_k)^T\mathbf{M}\mathbf{e}_k\geq 0, \tag{80}$$

where the vector $\mathbf{e}_k$ is defined in (76) and **n** represents the first column of **N**.

Proof. The first condition (I) represents the first equation from the Kalman-Szegö lemma; therefore, it is fulfilled (Landau, 1979).

In order to fulfil the second condition (II), the Popov inequality (80), which ensures the global asymptotic stability of the nonlinear CS for any positive constant β_0, is expressed:

$$S(k_1)=\sum_{k=0}^{k_1}(\mathbf{v}_k)^T\mathbf{y}_k\geq-\beta_0^2\ \ \forall k_1\in N^*. \tag{81}$$

Considering (76), the Popov sum $S(k_1)$ becomes:

$$S(k_1)=-\sum_{k=0}^{k_1}(\mathbf{u}_k)^T\mathbf{y}_k\ \ \forall k_1\in N^*. \tag{82}$$

By substituting in (82) the expression of $\mathbf{x}_{k+1}$ and $\mathbf{y}_k$ from (74), followed by adding and subtracting the term $(\mathbf{x}_{k+1})^T\mathbf{P}\cdot\mathbf{x}_{k+1}$ and using the properties of matrix transposition the Popov sum $S(k_1)$ becomes:

$$S(k_1)=-\sum_{k=0}^{k_1}\{-(\mathbf{x}_k)^T(\mathbf{A})^T\mathbf{P}\cdot\mathbf{A}\mathbf{x}_k-(\mathbf{x}_k)^T[(\mathbf{A})^T(\mathbf{P}++\mathbf{P}^T)\mathbf{B}+(\mathbf{C})^T]\mathbf{u}_k-(\mathbf{u}_k)^T(\mathbf{B})^T\mathbf{P}\cdot\mathbf{B}\cdot\mathbf{u}_k+(\mathbf{x}_{k+1})^T\mathbf{P}\cdot\mathbf{x}_{k+1}]\}\ \forall k_1\in N^*. \tag{83}$$

By replacing the expressions of $(\mathbf{A})^T\mathbf{P}\cdot\mathbf{A}$, $(\mathbf{A})^T\mathbf{P}^T\cdot\mathbf{B}$ and $(\mathbf{B})^T\mathbf{P}\cdot\mathbf{B}$ from the condition (I) and by expressing $\mathbf{x}_k$ from (77) and using the condition (II), another form of the Popov sum $S(k_1)$ is obtained:

$$S(k_1)=-\sum_{k=0}^{k_1}(\mathbf{x}_{k+1})^T\mathbf{P}\cdot\mathbf{x}_{k+1}+\sum_{k=0}^{k_1}[(\mathbf{e}_k)^T\mathbf{M}\cdot\mathbf{e}_k+(\mathbf{e}_k)^T\mathbf{N}\cdot\mathbf{u}_k+(\mathbf{u}_k)^T\mathbf{R}\cdot\mathbf{u}_k]\ \forall k_1\in N^*. \tag{84}$$

Using the expression of $\mathbf{u}_k$ in (76), (84) becomes:

$$S(k_1)=-\sum_{k=0}^{k_1}(\mathbf{x}_{k+1})^T\mathbf{P}\cdot\mathbf{x}_{k+1}+\sum_{k=0}^{k_1}[(\mathbf{e}_k)^T\mathbf{M}\cdot\mathbf{e}_k+(\mathbf{e}_k)^T\mathbf{N}\cdot\mathbf{F}(\mathbf{e}_k)+\mathbf{F}^T(\mathbf{e}_k)\mathbf{R}\cdot\mathbf{F}(\mathbf{e}_k)]\ \forall k_1\in N^*. \tag{85}$$

Finally, the expression of the sum $S(k_1)$ is obtained by using **F** from (73) and the positive element r_{11} of matrix **R**:

$$S(k_1)=-\sum_{k=0}^{k_1}[(\mathbf{x}_{k+1})^T\mathbf{P}\cdot\mathbf{x}_{k+1}+r_{11}f^2(\mathbf{e}_k)]+\sum_{k=0}^{k_1}[(\mathbf{e}_k)^T\mathbf{M}\cdot\mathbf{e}_k+f(\mathbf{e}_k)\mathbf{n}^T\cdot\mathbf{e}_k]\ \forall k_1\in N^*. \tag{86}$$

Both sums in (86) are positive and therefore the sum $S(k_1)$ is also positive, which means that the condition (II) guarantees the fulfilment of the Popov inequality (81). In conclusion, the fuzzy CS globally asymptotically stable, therefore Theorem 1 is proved.

For $n > 2$, only the matrix **P** from the first condition (I) is significant for the fuzzy CS stability analysis because the matrices **M**, **N** and **R** from the second condition (II) can be expressed as functions of **P**.

$$\mathbf{M}=-(\mathbf{C}^b)^T(\mathbf{A})^T\mathbf{P}\cdot\mathbf{A}\mathbf{C}^b,\ \mathbf{R}=-(\mathbf{B})^T\mathbf{P}\cdot\mathbf{B},\ \ \mathbf{N}=-(\mathbf{C}^b)^T[(\mathbf{A})^T(\mathbf{P}+\mathbf{P}^T)\mathbf{B}+(\mathbf{C})^T]. \tag{87}$$

Act 3.2 - The implementations, testing and validation of the new control structures with adaptive fuzzy control algorithms in industry with the support of one external partner. *(In Romanian – Implementarea, testarea și validarea noilor SRA cu regulatoare fuzzy adaptive în industrie prin intermediul unuia din partenerii din mediul privat).* Due to the pandemic period, no experiments could be done in the industry. Instead, extensive experiments were conducted in the team's laboratories. The published papers contain both simulation and real-time experimental results, which were validated on shape memory alloy (SMA) laboratory stands illustrated in Fig. 15 (Bojan-Dragos et al., 2022a; Precup et al., 2021c; Roman et al., 2022b; Roman et al., 2022c), but also on other laboratory equipment with SMA actuators, illustrated in Fig. 16, such as the vertical three tank system (Fig. 16 (a)) (Bojan-Dragos et al., 2022a), the tower crane system (Fig. 16 (b)) (Precup et al., 2022b; Precup et al., 2022c; Precup et al., 2022d; Roman et al., 2022a), the magnetic levitation system (Fig. 16 (c)) (Bojan-Dragos et al., 2022a), the electromagnetic actuated clutch system (Fig. 16 (d)) (Bojan-Dragos et al., 2021) and the modular servo system (Fig. 16 (e)) (Hedrea et al., 2021; Precup et al., 2021b; Precup et al., 2022a).

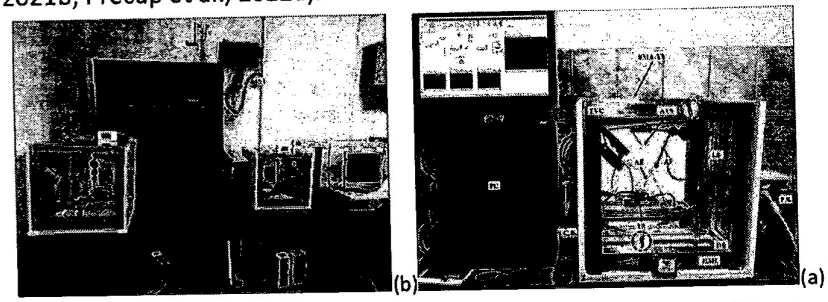
(b) (a)

Fig. 15. Laboratory equipment with SMA (a); Experimental arrangement of the SMA type laboratory stand (b).

The SMA laboratory equipment can be used for several test scenarios involving a wide range of sizes and shapes of SMA actuator-based elements, which are vital as the process has nonlinearities. Therefore, its tuning is a challenge for designers in the field of automatic control. The SMA laboratory equipment consists of a power supply (PS) that feeds five internal circuits to regulate at least one SMA-based Actuator each, an SMA test laboratory stand (SMA-TS) which is made of Aluminum Profile Frame, sensors, mechanical components that fulfill various mechanical implementations of SMA-based Actuators, and a personal computer, through which can regulate supply voltage and current limit protection and can be used as a cooling system to avoid unpleasant situations (Fig. 15 (a)). The communication between the SMA-TS and the PC is achieved by equipping the PC unit with a PCIe-6321 multi-functional I/O device (I/O D) of the PCI Express type with 16 AI (16-Bit, 250 kS/s), 2 AO (900 kS/s), 24 DIO, and its connection is also made through a 68-Pin Shielded

Connector Block cable that manages the hardware connections to the sensors and electronic switches.

Initially, this project started with a single laboratory stand, but during the project various parts and components were purchased that led to the development and improvement of the first shape memory alloys laboratory stand and the creation of the second stand according to Fig. 15 (b). The parameters of its mathematical model were optimally tuned using Takagi-Sugeno-Kang evolved fuzzy models (Precup et al., 2021c) and using the Grey Wolf Optimizer (GWO) algorithm (Bojan-Dragos et al., 2022b). Different types of adaptive fuzzy control algorithms were developed, implemented, tested and validated on real-world processes on the laboratory equipment with SMA with the support of the external partner from "Eftimie Murgu" University from Resita which is also in collaboration with „Babeș-Bolyai" University from Cluj-Napoca and on other laboratory equipment with SMA actuators with the support of the external partner from Ontario Centers of Excellence from Canada.

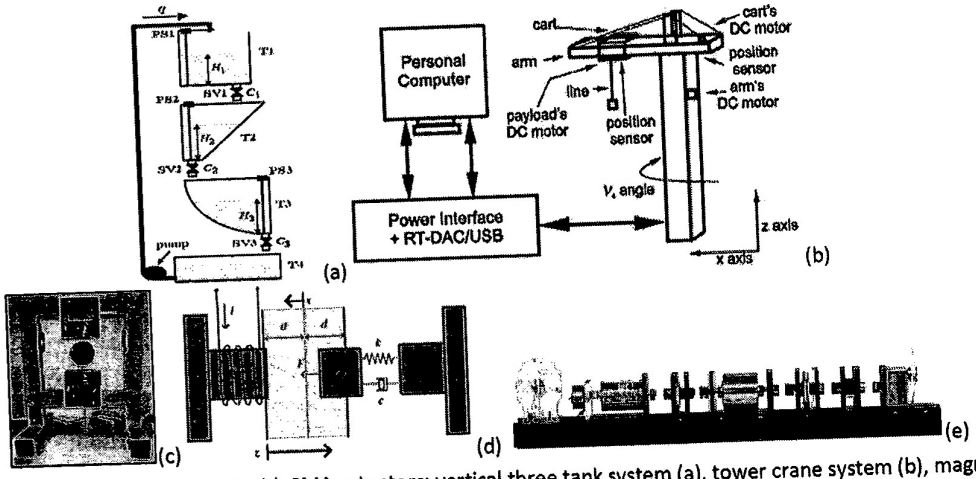

Fig. 16. Laboratory equipment with SMA actuators: vertical three tank system (a), tower crane system (b), magnetic levitation system (c), electromagnetic actuated clutch system (d), modular servo system (e)

Act 3.3 – Continuation and continuous improvement of collaboration with external industrial partners *(In Romanian – Continuarea și îmbunătățirea continuă a colaborării cu partenerii industriali externi).* To accomplish this activity, the team members participated to important conferences and self-critical discussions on the papers with partner research teams with similar activities. Although the funding period ends in the middle of September, the research team members will continue to publish papers that consist of the implementation, improvement and development of adaptive controllers with validations through simulations and experimental results on laboratory equipment related to SMA. From the research point of view, the achievements during the project involved the development of adaptive control algorithms regarding controlling processes that include Shape Memory Alloys (SMA) actuators and the implementation, testing and validation through simulations or experiments on real-world processes that include SMA or on the laboratory equipment with SMA with the support of the external partner from "Babes-Bolyai " University (the Resita Center) and on other laboratory equipment with SMA actuators with the support of the external partner, Emil M. Petriu, from Ontario Centres of Excellence (Precup et al., 2021a; Precup et al., 2021b; Precup et al., 2021c; Hedrea et al., 2021; Bojan-Dragos et al., 2022b; Precup et al., 2022a; Precup et al., 2022c; Precup et al., 2022d; Roman et al., 2022a; Roman et al., 2022c).

In the future, the new adaptive fuzzy control algorithms will also be validated through collaborations with industrial partners (Continental Automotive Timișoara, Airbus Helicopters Romania, as well as through direct scientific collaboration relationships consolidated over time, the Ontario Center of Excellence through the collective from within our department with the team from Ottawa, Canada within the University of Ottawa). The collaboration with the Canadian partner, Emil M. Petriu, is clearly highlighted by the completion of works (Precup et al., 2021a; Precup et al., 2021b; Precup et al., 2021c; Hedrea et al., 2021; Bojan-Dragos et al., 2022b; Precup et al., 2022a; Precup et al., 2022c; Precup et al., 2022d; Roman et al., 2022a; Roman et al., 2022c) from 2020 to 2022.

References

Alsayed, Y.M., Abouelsoud, A.A., Ahmed, M.R., and Bab, F.E. (2018). Fuzzy logic-based PI controller design and implementation of shape memory alloy actuator. International Journal of Automation and Control, 12 (3), 427-

448.
Andrianesis, K., Tzes, A. (2014). Development and control of a multifunctional prosthetic hand with shape memory alloy actuators. Journal of Intelligent and Robotic Systems, 78 (2), 257-289.

Åström, K.-J. and Hägglund, T. (1995). PID controllers theory: design and tuning. Instrument Society of America, Research Triangle Park.

Blazic, S., Skrjanc, I., Matko, D. (2014). A robust fuzzy adaptive law for evolving control systems, Evolving Systems, 5 (1), 3-10.

Bojan-Dragos, C.-A., Hedrea E.-L., Precup R.-E., Szedlak-Stinean A.-I., and Roman R.-C. (2019). MIMO fuzzy control solutions for the level control of vertical two tank systems. in Proc. 16th Int. Conf. Control, Autom. Robotics, Prague, Czech Republic, 1, 810–817.

Bojan-Dragoş, C.-A., Precup, R.-E., Preitl, S., Roman, R.-C., Hedrea, E.-L., and Szedlak-Stînean, A.-I. (2021). GWO-based optimal tuning of type-1 and type-2 fuzzy controllers for electromagnetic actuated clutch systems. IFAC-PapersOnLine, 54 (4), 189-194.

Dragoş, C.-A., Preitl, S., Precup, R.-E., Petriu, E. M., Stînean, A.-I. (2012). Adaptive control solutions for the position control of electromagnetic actuated clutch systems. In Proc. 2012 IEEE Intell. Vehicles Symp., Alcala de Henares, Spain, 81–86.

Castillo, O., Amador-Angulo, L., Castro, J.R., and García Valdez, M. (2016). A comparative study of type-1 fuzzy logic systems, interval type-2 fuzzy logic systems and generalized type-2 fuzzy logic systems in control problems. Information Sciences, 354, 257-274.

Castillo, O., Martinez-Marroquin, R., Melin, Valdez, P.F., and Soria, J. (2012). Comparative study of bio-inspired algorithms applied to the optimization of type-1 and type-2 fuzzy controllers for an autonomous mobile robot. Information Sciences, 192, 19-38.

Castillo, O. and Melin, P. (2014). A review on interval type-2 fuzzy logic applications in intelligent control. Information Sciences, 279, 615-631.

Castillo, O., Melin, P., Garza, A.A., Montiel, O., and Sepúlveda, R. (2011). Optimization of interval type-2 fuzzy logic controllers using evolutionary algorithms. Soft Computing, 15 (6), 1145-1160.

Di Cairano, S., Bemporad, A., Kolmanovsky, I.V., and Hrovat, D. (2007). Model predictive control of magnetically actuated mass spring dampers for automotive applications. International Journal of Control, 80 (1), 1701-1716.

Dominik, I. (2016). Type-2 fuzzy logic controller for position control of shape memory alloy wire actuator. Journal of Intelligent Material Systems and Structures, 27 (14), 1917-1926.

Hedrea, E.-L., Precup, R.-E., Bojan-Dragos, C.-A. (2019). Results on tensor product–based model transformation of magnetic levitation systems, Acta Polyt. Hung, 16, 93– 111.

Hedrea, E.-L., Precup, R.-E., Bojan-Dragos, C.-A. and Hedrea, C., (2019) Cascade control solutions for maglev systems, in Proc. 23nd ICSTCC, Sinaia, Romania, 20–26.

Hedrea, E.-L., Bojan-Dragos, C.-A., Precup, R.-E., Roman, R.-C., Petriu, E. M., & Hedrea, C. (2017). Tensor productbased model transformation for position control of magnetic levitation systems, in Proc. 26th Int. Symp. Ind. Electron., Edinburgh, UK, 1141–1146.

González, J., Gomáriz, S., Batlle, C., Galarza, C. (2015). Fuzzy controller for the yaw and velocity control of the Guanay II AUV, IFAC-PapersOnLine, 48(2), 268–273.

Guerra, T.-M., Sala, A., and Tanaka, K. (2015). Fuzzy control turns 50: 10 years later. Fuzzy Sets and Systems, 281, 168-182.

Ferdaus, M.M., Pratama, M., Anavatti, S.G., Garratt, M.A., and Lughofer E. (2020). PAC: A novel self-adaptive neuro-fuzzy controller for micro aerial vehicles. Information Sciences, 512, 481-505.

Kim, H.-J., Song, S.-H., and Ahn S.-H. (2013). A turtle-like swimming robot using a Smart Soft Composite (SSC) structure, Smart Materials and Structures, 22(1), 014007.

Keshtkar, N., Mersch, J., Katzer, K., Lohse, F., Natkowski, L., Gerlach, G., Zimmermann, M., Cherif, C., snf Robenack, K. (2021). Systems actuated by shape memory alloys: identification and modelling. System Theory, Control and Computing Journal, 1 (2), 1-9.

Kuang, Y., Miao, F., Liu, X., Xie, J., (2015). Experimental research and analysis of heating SMA wire, Proc. Int. Conf. on Ind. Techn. and Manag. Sci., 1162-1165.

Lagoudas, D.C. (Ed.) (2008). Shape Memory Alloys: Modeling and Engineering Applications. Springer Verlag, New York, NY.

Landau, I. D. (1979). Adaptive Control. New York: Marcel Dekker, Inc..

Lascu, C., Boldea, I., & Blaabjerg, F. (2013). Super-twisting sliding mode control of torque and flux in permanent magnet synchronous machine drives. IECON 2013 - 39th Annual Conference of the IEEE Industrial Electronics Society.

Lendek, Zs., Nagy, Z., Lauber, J. (2018). Local stabilization of discrete-time TS descriptor systems, Eng. Appl. Artif. Intell. J., 67, 409–418.

Levant, A., (1993). "Sliding order and sliding accuracy in sliding mode control", Int. Journal of Control, vol. 58,

no. 6, pp. 1247-1263.

Levant, A., (2003). "Higher-order sliding modes, differentiation and output feedback control", Int. Journal of Control, vol. 76, no. 9, pp. 924-941.

Levant, A., (2007). "Principles of 2-sliding mode design", Automatica, vol. 43, no. 4, pp. 576-586.

Levant, A., (2005). "Quasi-continuous higher-order sliding-mode controllers", IEEE Trans. Autom. Control, vol. 50, no. 11, pp. 1812-1816.

Quintanar-Guzmán, S., Kannan, S., Voos, H., Darouach, M., Alma, M. (2018). Adaptive control for a lightweight robotic arm actuated by a shape memory allow wire, Proc. 16th Internat. Conf. on New Actuat., Bremen, Germany, 388–393.

Matsumori, H., Deng, M.-C., and Noge Y. (2020). An operator-based nonlinear vibration control system using a flexible arm with shape memory alloy. International Journal of Automation and Control, 17 (1), 139-150.

Mendel, J.M. (2001). Uncertain rule-based fuzzy logic systems: Introduction and new directions. Prentice Hall PTR, Upper Saddle River, NJ.

Mittal, K., Jain, A., Singh Vaisla, K., Castillo, O., and Kacprzyk, J. (2020). A comprehensive review on type 2 fuzzy logic applications: Past, present and future. Engineering Applications of Artificial Intelligence, 95, 103916.

Mituletu, I.-C., Bizau, V.I., Chioncel, C.P., and Gillich, G.R. (2019). The design of a test stand for the shape memory alloys control at high current and low voltage. Proceedings of XIth International Symposium on Advanced Topics in Electrical Engineering, Bucharest, Romania, 1-6.

Mohd Jani, J., Leary, M., Subic, A., Gibson, M. A. (2014). A review of shape memory alloy research, applications and opportunities, Mater. Des., 56, 1078–1113.

Nguyen, A.-T., Taniguchi, T., Eciolaza, L., Campos, V., Palhares, R., Sugeno, M. (2019). Fuzzy control systems: past, present and future, IEEE Computational Intelligence Magazine, 14(1), 56–68.

Phan, D., Bab-Hadiashar, A., Fayyazi, M., Hoseinnezhad, R., Jazar, R.N., and Khayyam, H. (2020). Interval type-2 fuzzy logic control for energy management of hybrid electric autonomous vehicles. IEEE Transactions on Intelligent Vehicles, 2020, DOI: 10.1109/TIV.2020. 3011954.

Popov, V. M. (1973). Hyperstability of Control Systems, Berlin, Heidelberg, New York, Springer-Verlag.

Pozna, C. and Precup, R.-E., An approach to the design of nonlinear state-space control systems. (2018). Stud. Informat. Control, 27 (1), 5-14.

Precup, R.-E., Bojan-Dragoş, C.-A., Hedrea, E.-L., Roman, R.-C., and Petriu, E. M. (2021). Evolving fuzzy models of shape memory alloy wire actuators. Romanian Journal of Information Science and Technology, 24 (4), 1-13.

Precup, R.-E., Tomescu, M.-L., and Dragos, C.-A. (2014) Stabilization of Rössler chaotic dynamical system using fuzzy logic control algorithm. Int. J. Gen. Syst., 43 (5), 413-433.

Precup, R.-E., Angelov, P., Costa, B.S.J., and Sayed-Mouchaweh, M. (2015). An overview on fault diagnosis and nature-inspired optimal control of industrial process applications. Computers in Industry, 74, 75-94.

Precup, R.-E. and David. R.-C. (2019). Nature-inspired optimization algorithms for fuzzy controlled servo systems. Butterworth-Heinemann, Elsevier, Oxford.

Precup, R.-E., David, R.-C., and Petriu, E.M. (2017a). Grey wolf optimizer algorithm-based tuning of fuzzy control systems with reduced parametric sensitivity. IEEE Transactions on Industrial Electronics, 64 (1), 527-534.

Precup, R.-E., David, R.-C., Petriu, E.M., Szedlak-Stinean, A.-I., and Bojan-Dragos, C.-A. (2016). Grey wolf optimizer-based approach to the tuning of PI-fuzzy controllers with a reduced process parametric sensitivity. IFAC-PapersOnLine, 49 (5), 55-60.

Precup, R.-E., David, R.-C., Szedlak-Stinean, A.-I., Petriu, E.M., and Dragan, F. (2017b). An easily understandable grey wolf optimizer and its application to fuzzy controller tuning. Algorithms, 10 (2), 68.

Precup, R.-E. and Preitl, S., (1997). Popov-type stability analysis method for fuzzy control systems, in Proc. Fifth Europ. Congr. Intell. Tech. Soft Comp., Aachen, Germany, 2, 1306-1310.

Precup, R.-E. and Preitl, S., (2003). Popov-type stability analysis method for fuzzy control systems with PI fuzzy controllers, Rev. Roum. Sci. Tech. Electr. Ener. Ser., 48 (4), 505-522.

Precup, R.-E.; Preitl, S. (2006). Stability and sensitivity analysis of fuzzy control systems. Mechatronics applications, Acta Polytechnica Hungarica, 3(1), 61–76, 2006

Precup, R.-E., Preitl, S., Petriu, E. M., Roman, R.-C., Bojan-Dragoş, C.-A., Hedrea, E.-L., and Szedlak-Stînean, A.-I. (2020). A center manifold theory-based approach to the stability analysis of state feedback Takagi-Sugeno-Kang fuzzy control systems, Facta Universitatis, Series: Mechanical Engineering (University of Nis), 18 (2), 189-204.

Precup, R.-E., Tomescu, M.-L., Dragoş, C.-A. (2014). Stabilization of Rössler chaotic dynamical system using fuzzy logic control algorithm, Int. J. Gen. Syst., 43(5), 413–433.

Precup, R.-E., Preitl, S., Solyom, S., (1999). Center manifold theory approach to the stability analysis of fuzzy control systems, in Computational Intelligence. Theory and Applications, Reusch, B., Ed., Springer-Verlag, Berlin, Heidelberg, New York, Lecture Notes in Computer Science, 1625, 382-390.

Precup, R.-E., Teban, T.-A., Albu, A., Borlea, A.-B., Zamfirache, I.A., Petriu, E.M. (2020). Evolving fuzzy models for

prosthetic hand myoelectric-based control. IEEE Transactions on Instrumentation and Measurement, 69 (7), 4625-4636.

Raja, R., Mohan, B. M. (2018). Stability Analysis of General Takagi-Sugeno Fuzzy Two-Term Controllers, Fuzzy Inf. Eng. J., 10(2), 196–212.

Taghavifar, H. and Rakheja, S. (2019). Path-tracking of autonomous vehicles using a novel adaptive robust exponential-like-sliding-mode fuzzy type-2 neural network controller. Mechanical Systems and Signal Processing, 130, 41-55.

Shamloo, N.F.; Kalat, A.A.; Chisci, L. (2020). Indirect adaptive fuzzy control of nonlinear descriptor systems, European Journal of Control, 51, 30–38, 2020.

Zhang, B., Zhao, X.-G., Li, X.-G., Zhang, D.-H. (2018). Robust indirect adaptive control for a class of nonlinear systems and its application to shape memory alloy actuators, IEEE Access, 6, 35809– 35823.

Senthilkumar, M. (2012). Analysis of SMA actuated plain flap wing, Journ. of Engineer. Sci. and Technol. Review vol. 5(1), 39-43.

Senthilkumar, P., Umapathy, M., Dhanalakshmi, K. (2014). Modulated adaptive fuzzy controller for position control of SMA wire actuator, J. Intell. Fuzzy Syst., 27(1), 9–18.

Soother, D.K., Daudpoto, J., and Chowdhry, B.S. (2020). Challenges for practical applications of shape memory alloy actuators. Materials Research Express, 7 (7), 073001.

Suhel, K., Sai, Y., Mani Prabu, S.S., Palani, I.A., Amod, C.U., and Singh, P. (2018). Active control of smart shape memory alloy composite flapper for aerodynamic applications. Procedia Computer Science, 133, 134-140.

Yang, H., Xu, M., Li, W., and Zhang, S. (2019). Design and implementation of a soft robotic arm driven by SMA coils. IEEE Transactions on Industrial Electronics, 66 (8), 6108-6116.

B. Prezentarea rezultatelor obținute, a indicatorilor de rezultat realizați; a nerealizărilor înregistrate față de rezultatele estimate prin cererea de finanțare (dacă este cazul), cu justificarea acestora;

The main results obtained in the 1st Stage of the project:

- **1 accepted paper** to be published in Clarivate Analytics Web of Science (formerly ISI Web of Knowledge) journals with impact factors (Precup et al., 2021a): this paper was published in 2021 and it is passed in the main results obtained in the 2nd Stage of the project.
- **1 scientific report.**

The main results obtained in the 2nd Stage of the project:

- **2 papers** published in Clarivate Analytics Web of Science (formerly ISI Web of Knowledge) journals with impact factors (Precup et al., 2021a; Precup et al., 2021b): A combination of the model-free control technique with two popular nonlinear control techniques, sliding mode control and fuzzy control are designed and validated in (Precup et al., 2021a) by real-time experiments conducted on 3D crane system laboratory equipment; Optimal tuning of cost-effective fuzzy controllers represented by Takagi–Sugeno–Kang proportional-integral fuzzy controllers (TSK PI-FCs) is carried out using a fresh metaheuristic algorithm, namely the Slime Mould Algorithm (SMA), and a fuzzy controller tuning approach is offered in (Precup et al., 2021b).
- **1 paper** accepted to be published in Clarivate Analytics Web of Science (formerly ISI Web of Knowledge) journals with impact factors (Precup et al., 2021c): this paper suggests Takagi-Sugeno-Kang (TSK) fuzzy models that characterize the position of Shape Memory Alloy (SMA) wire actuators.
- **2 papers** published in conference proceedings indexed in Clarivate Analytics Web of Science (formerly ISI Web of Knowledge) (Bojan-Dragos et al., 2021; Hedrea et al., 2021): A Takagi-Sugeno type-1 fuzzy logic controller and a Takagi-Sugeno type-2 fuzzy logic controller are optimally tuned in (Bojan-Dragos et al., 2021) using metaheuristic Grey Wolf Optimizer algorithm to enhance position tracking performance of electromagnetic actuated clutch systems with SMA actuators, which are subjected to parametric; A Tensor Product (TP)-based model of a family of nonlinear servo systems, whose parameters were optimally tuned using a metaheuristic Grey Wolf Optimizer algorithm, was design and validated in (Hedrea et al., 2021).
- **1 paper** presented in conference proceedings to be indexed in international databases (IEEE Xplore, INSPEC, Scopus, DBLP) (Roman et al., 2022a): this paper was published in 2022 and it is passed in the main results obtained in the 3rd Stage of the project.
- **1 scientific report.**

The main results obtained in the 3rd Stage of the project:

- cumulated impact factor according to 2021 Journal Citation Reports (JCR) released by Clarivate Analytics in 2022 = 8.109,

- **1 book** (Bojan-Dragos et al., 2022a): Mamdani or Takagi-Sugeno fuzzy controllers and combined adaptive fuzzy controllers (gain-scheduling fuzzy controllers, optimal fuzzy controllers, two degree of fredam fuzzy controllers, sliding mode fuzzy controllers) were developed in this book to control the sphere position of a magnetic levitation system with SMA actuators, to control the position of an electromagnetic actuated clutch system with SMA actuators, to control the liquid level in three tanks systems with SMA actuators and to control the speed of a vehicle with continuously variable transmission and SMA actuators;

- **2 papers** published in Clarivate Analytics Web of Science (formerly ISI Web of Knowledge) journals with impact factors (Precup et al., 2022a; Precup et al., 2022b, Szedlak Stinean et al., 2022): Data-Driven Fuzzy Control approach was proposed in (Precup et al., 2022a) for the position control of a nonlinear servo system with SMA actuators; the performance improvement of three Single Input-Single Output (SISO) fuzzy control systems to control separately the cart position, the arm angular position and the payload position of a tower crane systems with SMA actuators is preseted in (Precup et al., 2022b).

- **1 paper** accepted to be published in Clarivate Analytics Web of Science (formerly ISI Web of Knowledge) journals with impact factors (Szedlak Stinean et al., 2022): Two nonlinear estimation approaches, namely based on Extended Kalman Filter (EKF) and a Takagi-Sugeno Fuzzy Observer with 32 rules (TSFO-32), for a Strip Winding System (SWS) characterized by variable reference input, variable moment of inertia with constant increasing tendency and variable parameters.

- **1 paper** published in conference proceedings indexed in Clarivate Analytics Web of Science (formerly ISI Web of Knowledge) (Roman et al., 2022a): Iterative Feedback Tuning (IFT) algorithm is proposed in this paper to control the cart position, the arm angular position and the payload position of a tower crane systems with SMA actuators.

- **5 papers** presented in conference proceedings to be indexed in international databases (IEEE Xplore, INSPEC, Scopus, DBLP) (Bojan-Dragos et al., 2022b; Precup et al., 2022c; Precup et al., 2022d; Roman et al., 2022b; Roman et al., 2022c): Two Proportional-Integral-Derivative controllers, a type-1 fuzzy controller and an interval type-2 fuzzy controller are optimally tuned in (Bojan-Dragos et al., 2022b) using metaheuristic Grey Wolf Optimizer algorithm to control the nonlinear processes with Shape Memory Alloy (SMA) wire actuators, the African Vultures Optimization Algorithm (AVOA)-based tuning of low-cost fuzzy controllers (first order discrete-time intelligent Proportional-Integral controllers with Takagi-Sugeno-Kang Proportional-Derivative fuzzy terms) is proposed in (Precup et al., 2022c) to control the payload position of tower crane systems with SMA actuators; Three cost-effective SISO fuzzy controllers as first order discrete time intelligent Proportional-Integral (PI) controllers with Takagi-Sugeno-Kang Proportional-Derivative (PD) fuzzy terms are included in three SISO current iteration Iterative Learning Control (ILC) system structures with PD-type learning rules and are implemented in (Precup et al., 2022d) to control the cart position, the arm angular position and the payload position of tower crane systems with SMA actuators; Three data-driven control algorithms, namely Active Disturbance Rejection Control, Model-Free Adaptive Control and Model Free Control are optimally tuned in terms of solving an optimization problem in (Roman et al., 2022b) to the position control of shape memory alloy; The paper (Roman et al., 2022c) proposes to compare the performances of a proportional-integral controller whose parameters are determined in a model-based way using a metaheuristic search algorithm, with the performances of a PI determined in a mode-free way by using virtual reference feedback tuning algorithm and using iterative feedback tuning algorithm to control the position of a shape memory alloy (SMA) laboratory equipment;

- **1 scientific report.**

Remarks:

- Some of the papers presented in Section C contain more than one project in the Acknowledgements section. Several projects contributed to the creation of these papers because the same processes are controlled, different controllers developed in different projects were proposes, and their fair comparison was necessary.
- All published papers or accepted to be published which contains research results obtained under this project mentioned the support of UEFISCDI in the Acknowledgments section, together with the specification of the submitting code of the funding application.
- The obtained results are also mentioned in the web page of the project, http://www.aut.upt.ro/~claudia.dragos/TE2019.html, where all the information related to the development of the project will be included.

C. Impactul estimat al rezultatelor obținute, cu sublinierea celui mai semnificativ rezultat obținut.

The main results obtained in the project:

- cumulated impact factor according to 2021 Journal Citation Reports (JCR) released by Clarivate Analytics in 2022 = 12.781,

- ***Books:***

Bojan-Dragoş, C.-A., Precup, R.-E., Hedrea, E.-L. (2022a). Sisteme de reglare fuzzy cu aplicatii mecatronice, Editura Politehnica, Colectia Automatica, pp. 166, ISBN 978-606-35-0472-3.

- ***Journal Papers:***

Precup, R.-E., Roman, R.-C., Hedrea, E.-L., Petriu, E. M. and Bojan-Dragoş, C.-A. (2021a). Data-Driven Model-Free Sliding Mode and Fuzzy Control with Experimental Validation, International Journal of Computers Communications & Control (Agora University Editing House - CCC Publications), 16 (1), 4076, 1-17, impact factor (IF) = 2.293, IF according to 2021 Journal Citation Reports (JCR) released by Clarivate Analytics in 2022 = 2.635 (univagora.ro/jour/), 4 independent citations according to Clarivate Analytics Web of Science.

Precup, R.-E., David, R.-C., Roman, R.-C., Petriu, E. M., Szedlak-Stinean, A.-I. (2021b). Slime Mould Algorithm-Based Tuning of Cost-Effective Fuzzy Controllers for Servo Systems, International Journal of Computational Intelligence Systems, 14 (1), 1042–1052, impact factor (IF) = 1.736, IF according to 2021 Journal Citation Reports (JCR) released by Clarivate Analytics in 2022 = 2.259, 28 independent citations according to Clarivate Analytics Web of Science.

Precup, R.-E., Bojan-Dragoş, C.-A., Hedrea, E.-L., Roman, R.-C., Petriu, E. M. (2021c). Evolving Fuzzy Models of Shape Memory Alloy Wire Actuators, Romanian Journal of Information Science and Technology (Romanian Academy, Section for Information Science and Technology), 24 (4), pp. 353-365, impact factor (IF) = 0.643, IF according to 2021 Journal Citation Reports (JCR) released by Clarivate Analytics in 2022 = 0.852, 4 independent citations according to Clarivate Analytics Web of Science.

Precup, R.-E., Preitl, S., Bojan-Dragos, C.-A., Hedrea, E.-L., Roman R.-C., Petriu, E. M. (2022a) A Low-Cost Approach to Data-Driven Fuzzy Control of Servo Systems," Facta Universitatis, Series: Mechanical Engineering, 20 (1), pp. 021-036, impact factor (IF) = 4.622, IF according to 2021 Journal Citation Reports (JCR) released by Clarivate Analytics in 2022 = 4.622, 1 independent citations according to Google Scholar.

Precup, R.-E., Roman, R.-C., Hedrea, E.-L., Bojan-Dragos, C.-A., Damian, M.-M., Nedelcea, M.-L. (2022b). Performance Improvement of Low-Cost Iterative Learning-Based Fuzzy Control Systems for Tower Crane Systems, International Journal of Computers Communications & Control, 17 (1), pp. 1-18, impact factor (IF) = 2.635, IF according to 2021 Journal Citation Reports (JCR) released by Clarivate Analytics in 2022 = 2.635, 2 independent citations according to Clarivate Analytics Web of Science.

Szedlak Stinean, A.-I., Precup, R.-E., Petriu, E. M., Roman, R.-C., Hedrea, E.-L., Bojan-Dragos, C.-A. (2022). Extended Kalman filter and Takagi-Sugeno fuzzy observer for a strip winding system, accepted to be publisehd in Expert Systems with Applications, vol. 208, pp. 118-215, impact factor (IF) = 8.665, IF according to 2021 Journal Citation Reports (JCR) released by Clarivate Analytics in 2022 = 8.665.

- ***Conference Proceedings papers***

Bojan-Dragos, C.-A., Precup, R.-E., Petriu, E. M., Roman, R.-C., Hedrea, E.-L., Szedlak Stinean, A.-I. (2022b). GWO-Based Optimal Tuning of Controllers for Shape Memory Alloy Wire Actuators, 6th IFAC Conference on Intelligent Control and Automation Sciences, Cluj-Napoca, Romania, pp. 1-6.

Bojan-Dragoş, C.-A., Precup, R.-E., Preitl, S., Roman, R.-C., Hedrea, E.-L. and Szedlak-Stînean, A.-I. (2021). GWO-Based Optimal Tuning of Type-1 and Type-2 Fuzzy Controllers for Electromagnetic Actuated Clutch Systems, Proceedings of 4th IFAC Conference on Embedded Systems, Computational Intelligence and Telematics in Control CESCIT 2021, Valenciennes, France, 2021, IFAC-PapersOnLine, 54 (4), 189-194, indexed in Scopus, 17 independent citations according to SCOPUS and 22 independent citations according to Google Scholar.

Hedrea, E.-L., Precup, R.-E., Roman, R.-C., Petriu, E. M., Bojan-Dragoş, C.-A. and Hedrea, C. (2021). Tensor Product-Based Model Transformation Technique Applied to Servo Systems Modeling, Proceedings of 30th International Symposium on Industrial Electronics ISIE 2021, Kyoto, Japan, 1-6, indexed in IEEE Xplore.

Precup, R.-E., Hedrea, E.-L., Roman, R.-C., Petriu, E. M., Bojan-Dragos, C.-A., Szedlak Stinean, A.-I., Paulescu, F.-A. (2022c). AVOA-Based Tuning of Low-Cost Fuzzy Controllers for Tower Crane Systems, 2022 IEEE International Conference on Fuzzy Systems (FUZZ-IEEE), Padova, Italy, pp. 1-6.

Precup, R.-E., Hedrea, E.-L., Roman, R.-C., Petriu, E. M., Bojan-Dragos, C.-A., Szedlak Stinean, A.-I. (2022d). GWO-Based Performance Improvement of PD-Type Iterative Learning Fuzzy Control of Tower Crane Systems, 2022 IEEE International Symposium on Industrial Electronics, Anchorage, AK, USA, pp. 1-6.

Roman, R.-C., Precup, R.-E., Hedrea, E.-L., Preitl, S., Zamfirache, I. A., Bojan-Dragos, C.-A., Petriu, E. M. (2022a). Iterative Feedback Tuning Algorithm for Tower Crane Systems, Procedia Computer Science, 199, pp. 157-165.

Roman, R.-C., Precup, E.-L., Preitl, S., Bojan-Dragos, C.-A., Szedlak Stinean, A.-I., Hedrea, E.-L. (2022b). Data-Driven Control Algorithms for Shape Memory Alloys, 6th IEEE Conference on Control Technology and Applications, Trieste, Italy, pp. 1-7.

Roman, R.-C., Precup, R.-E., Preitl, S., Szedlak Stinean, A.-I., Bojan-Dragos, C.-A., Hedrea, E.-L., Petriu, E.-L. (2022c). PI Controller Tuned via Data-Driven Algorithms for Shape Memory Alloy Systems, 1st IFAC Workshop on Control of Complex Systems, COSY 2022, Bologna, Italy, pp. 1-6.

Director Proiect,

BOJAN-DRAGOŞ Claudia-Adina